Icarus **150**, 104–123 (2001)
doi:10.1006/icar.2000.6568, available online at http://www.idealibrary.com on IDEAL®

Mean Motion Resonances in the Transneptunian Region

Part II: The 1 : 2, 3 : 4, and Weaker Resonances

D. Nesvorný[1] and F. Roig

Institute of Astronomy and Geophysics, São Paulo University, Av. Miguel Stefano 4200, 04301 São Paulo, SP, Brazil
E-mail: david@obs-nice.fr

Received February 16, 2000; revised October 16, 2000

The stability of orbits in the transneptunian region is numerically computed. It is found that, in analogy to the asteroid belt, there exist many chaotic layers associated with thin mean-motion resonances. These are either moderate- and high-order resonances with Neptune or three-body resonances with Neptune and Uranus. The orbital eccentricity chaotically increases at the thin resonances, allowing some Kuiper Belt objects to be slowly transferred to Neptune-crossing orbits. The stability of two large mean-motion resonances with Neptune, the 1 : 2 and 3 : 4, is systematically explored. It is shown that orbits in both resonances, with small resonant amplitudes are stable over the age of the Solar System. The possible role of collisions and dynamical scattering in clearing the resonances is discussed. It is inferred from orbital angles of 1997 SZ10 and 1996 TR66 that these bodies are most probably on stable tadpole orbits in the 1 : 2 Neptune resonance.

Key Words: **Kuiper Belt; Oort Cloud, celestial mechanics; stellar dynamics.**

1. INTRODUCTION

This paper extends our previous work, in which the regular and chaotic dynamics of the 2 : 3 mean-motion resonance (MMR) with Neptune was studied (Nesvorný and Roig 2000; hereafter N&R00). In N&R00, we calculated the maximum Lyapunov characteristic exponent (LCE) and measures of chaotic evolution of orbital elements (Laskar 1994, Morbidelli 1996) and frequencies (Laskar 1999) for initial conditions on a grid in a, e, i. The first set of initial conditions (1010 orbits) sampled the 2 : 3 resonant orbits at low inclinations and the second set (405 orbits) included large-inclination orbits. We have classified the resonant orbits into three groups: (i) those for which the escape rate to Neptune-crossing orbits at $t = 4$ Byr was more than 1% of the initial population per 1 Byr.[2] We called these orbits the *marginally unstable* orbits. Other orbits, i.e., those for which the escape rate at $t = 4$ Byr was less than 1%, were either (ii) *strongly unstable* orbits, where most of the original population escaped at $t < 4$ Byr, so that at $t = 4$ Byr there were too few surviving bodies to assure the required flux, or (iii) *practically stable* orbits, with the dynamical lifetimes largely exceeding the age of the Solar System and an equally negligible escape rate at $t = 4$ Byr.

The practically stable orbits were characterized by a small LCE and very slow chaotic evolution, and were usually located in the core of the 2 : 3 Neptune MMR. The marginally unstable orbits had larger LCEs (10^{-5}–10^{-6} yr^{-1}) and were initially located at larger resonant amplitudes ($A_\sigma \sim 100^\circ$–120°), where the slow chaotic evolution of A_σ transferred them, after a long time interval, to the strongly unstable region at the resonant borders. The strongly unstable orbits had initially $A_\sigma > 120^\circ$–130° and their A_σ quickly increased, driving them outside the resonance, where bodies lose phase protection against the encounters with Neptune.

This resonant structure has been already known (Duncan *et al.* 1995, Morbidelli 1997, Gallardo and Ferraz-Mello 1998) N&R00 provided an understanding of the 2 : 3 MMR dynamics that is both detailed and global. We identified several secular and other mechanisms present inside the resonance that have a nonnegligible effects on the orbital chaos and instability of resonant objects.

In N&R00, we also discussed the observed population of the 2 : 3 Neptune MMR (Pluto and 15 Plutinos with well-determined orbits) and its relation to the Jupiter-family comets. Assuming that the 2 : 3 MMR supplies 15% of new comets needed to keep the population of the Jupiter-family comets in a steady state, we computed that at most 6×10^8 comets currently exist in the resonance.

[1] Present address: Observatoire de la Côte d'Azur, BP 4229, 06304 Nice Cedex 4, France.

[2] If $P(t)$ is the percentage of test particles escaping from the initial population in the interval $[0, t]$, then by the escape rate at time t we mean the derivative of this function. For practical reasons, we refer here and in the following to the escape rate in units of per billion years.

0019-1035/01 $35.00

In modeling the chaotic dynamics in N&R00 we used special numerical methods. The chaotic evolution (diffusion) was measured by the change of frequencies (frequency analysis) and of actions (determined as extrema of filtered orbital elements on a time-shifting window) over 45 Myr. The algorithms were described in N&R00 and we refer the reader to Section 3.2 of that paper.

One of the recent accomplishments achieved by the application of the above methods was in understanding the fine structure of the asteroid belt. It turned out that, besides the main mean-motion and secular resonances, there exist a large number of thin ($<10^{-2}$ AU) chaotic layers associated with moderate- and high-order MMRs with Jupiter (Holman and Murray 1996), three-body resonances with Jupiter and Saturn (Nesvorný and Morbidelli 1998, 1999), or exterior MMRs with Mars (Morbidelli and Nesvorný 1999). About 40% of asteroids are strongly chaotic and have the Lyapunov time (inverse of the LCE) less than 10^5 yr (Šidlichovský and Nesvorný 1999) because they are located in some thin MMR. Although the chaotic changes of eccentricity that drive resonant asteroids to planet-crossing trajectories happen on much longer time intervals, the stability over the age of the Solar System is not assured for many of them (Murray and Holman 1997, Migliorini *et al.* 1998). As we describe in Section 2, the situation in the Kuiper Belt (KB) is similar.

A detailed account of an extensive literature about the KB dynamics was given in N&R00. In brief, Duncan *et al.* (1995) computed a detailed map of stable/unstable regions in the KB by integrating a large number of orbits in the 32–50 AU semi-major axis interval. The orbits starting at perihelion distances less than 35 AU were found unstable in 4 Byr unless they were associated to some Neptune MMR (Morbidelli *et al.* 1995, Malhotra 1995, Morbidelli 1997). The orbits with the perihelion distances larger than 35 AU were found stable unless they were related to the perihelion or node secular resonances (Knežević *et al.* 1991). These findings determined the stable locations in the KB where real Kuiper Belt objects (KBOs) Could remain today. Indeed, most of the 300 comets detected at present in the KB are located in the stable regions found by Duncan *et al.* (1995). It also turned out that some of the stable regions found by Duncan *et al.* are not populated. This is the main argument that something besides the dynamical sculpting of the planets is responsible for the structure we see. The reader can refer to the review of Morbidelli (1998) for further reading on the Kuiper Belt primordial evolution and its present dynamics.

In this paper we also investigate the regular and chaotic dynamics of two large MMRs. In Section 3 we study the stability of the 1 : 2 MMR with Neptune at 47.8 AU. It is interesting to know whether this resonance is unstable over the age of the Solar System or whether the lack of observed resonant bodies (we discuss the orbits of two possible candidates for 1 : 2 MMR KBOs—1996 TR66 and 1997 SZ10—in Section 3.1) is related to some primordial mechanism. Even if Duncan *et al.* 1995) already showed that there exist some stable 1 : 2 resonant orbits, We believe that a detailed anlysis is needed to answer this question with more confidence.

The 1 : 2 and 2 : 3 Neptune MMRs should have been initially populated by an approximately equal number of objects in the scenario of smooth expansion of the planetary orbits with adiabatic capture of objects into resonances (Malhotra 1995). Hahn and Malhotra (1999) have shown that the above is not necessarily true if the planets interacted with a massive primordial disk ($\sim 50\ M_\oplus$). In this case, the semi-major axis of Neptune was subject to random kicks that made the captures in the 1 : 2 MMR inefficient. Moreover, the scenario of excitation and mass loss in the primordial KB driven by Neptune-scattered planetesimals (Petit *et al.* 1999) does not favor the resonant populations with respect to the nonresonant ones. In Section 3.3, we show what ratio of the 1 : 2 and 2 : 3 MMR populations should be expected from the respective sizes of the stable resonant cores.

In Section 4 we extend the present analysis to the 3 : 4 MMR with Neptune at 36.5 AU, where one KBO—1995 DA2—with well-determined orbit is found. This resonance was proved to be stable over the age of the Solar System by Duncan *et al.* (1995), who also showed that the chaotic evolution on the limit of the stable core of the 3 : 4 MMR mostly affects A_σ.

2. THE FINE RESONANT STRUCTURE OF THE TRANSNEPTUNIAN REGION

The initial conditions of 2800 test particles were chosen equidistantly spaced in semi-major axis ($\Delta a = 0.004$ AU) between 38.8 and 50 AU, fixing $e = 0.1$ and $i = \lambda = \varpi = \Omega = 0$, where λ, ϖ, and Ω are the mean, perihelion and node longitudes, respectively. The initial conditions of four outer planets (Jupiter to Neptune) with respect to the mean ecliptic and equinox J2000 were taken from the JPL DE403 ephemeris for the date 2/21/1997 (JD 2450500.5). The orbital evolution of massive bodies (planets) and massless test particles were computed by the symmetric multistep integrator (Quinlan and Tremaine 1990) for 10^8 yr using a 40-day step for the planets and a 200-day step for the test particles. Additionally, the variational equations were numerically integrated for the purpose of the LCE evaluation of each simulated orbit. This was done by the symmetric multistep method using the same step sizes. The variational vector was periodically renormalized following the algorithm of Benettin *et al.* (1976) in order to avoid computer overflow. The LCE estimate for each surviving test particle was computed as $\ln \Delta(t)/t$, with $t = 10^8$ yr ($\Delta(t)$ is the norm of the variational vector at time t), and is plotted as a function of the initial semi-major axis in Fig. 1c. For the test particles escaping to Neptune-crossing orbits, $\ln \Delta(t)/t$ was plotted at the time of the first Neptune crossing. The minimum value of the LCE that we can detect with the integration time span is about 10^{-7} yr^{-1}. Examples of regular, moderately, and strongly chaotic trajectories as well as the interpretation of the LCE dependence on the semi-major axis were discussed in Morbidelli and Nesvorný (1999).

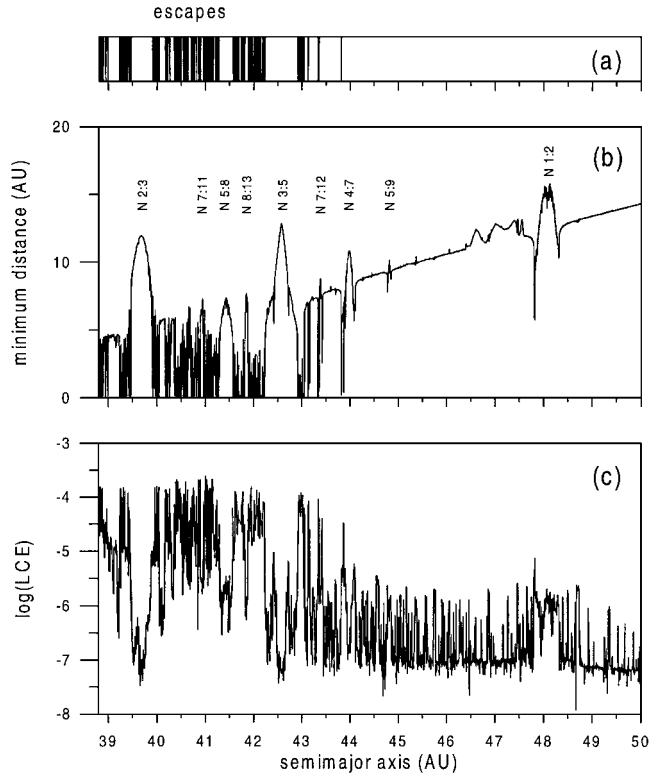

FIG. 1. A survey of LCEs in the transneptunian region: (a) a vertical line was placed at the initial a if the corresponding test particle escaped at $t < 10^8$ yr; (b) minimum distances of test particles to Neptune; and (c) LCE estimates at $t = 10^8$ yr (in logarithmic scale). The initial e and i of the 2800 integrated test particles were 0.1 and 0°, respectively. The test particles at MMRs with Neptune have their minimum distance (b) larger than the test particles in the immediate vicinity due to the resonant phase-protection mechanism. Apart from the main resonances, which may be easily identified in (c) as wide "holes" and "peaks," there are many thin peaks for $a > 44$ AU with the LCE ranging from 10^{-6} to 10^{-7} yr^{-1}. These peaks are related to thin MMRs with Neptune and Uranus. Note the rough background profile of the LCE at about 10^{-7} yr^{-1} for $a > 44$ AU, suggesting the stochasticity of all the integrated trajectories.

2.1. The Phase-Protection Mechanism in MMRs

The minimum-approach distance of each test particle to Neptune in 10^8 yr is plotted in Fig. 1b. The vertical line in Fig. 1a denotes the initial a of test particles that attained the Neptune-crossing orbits in the integrated time span; these orbits were usually ejected to heliocentric distances larger than 100 AU.

More than 50% of test particles with initial $a < 43$ AU escaped to Neptune-crossing orbits. Those that survived in this semi-major axis interval were the test particles that avoided encounters with Neptune, being locked in MMRs (labeled in Fig. 1b). This is easily seen (Fig. 1b) for the 2 : 3, 7 : 11, 5 : 8, 8 : 13, and 3 : 5 MMRs, in which the minimum distance to Neptune is kept larger than in the background.

The phase-protection mechanism is a consequence of resonant dynamics. The resonant angle σ of the $p+q:p$ MMR with Neptune is defined by

$$q\sigma_{p+q:p} = -(p+q)\lambda_{\rm N} + p\lambda + q\varpi, \qquad (1)$$

where p, q are integers and $\lambda_{\rm N}$ is the mean longitude of Neptune. $q \geq 1$ is called the order of the resonance, and the width of the resonance in a is generally proportional to the power $q/2$ of the eccentricity. For the resonances interior to the planet's orbit, $p \geq 1$, and for the outer resonances, $p \leq -2$. With exception of the MMRs with $p+q=-1$ and $p \leq -2$ (i.e., the outer resonances of the type $1:r$, $r \geq 2$), which permit asymmetric librations (Beaugé 1994), the angle $q\sigma_{p+q:p}$ oscillates either about 0° (inner resonances with q odd) or 180° (inner resonances with q even, and outer resonances with $p+q \neq -1$).

Assuming a body to be locked in some outer resonance ($p \leq -2$) with the libration center at 180° and a circular orbit for the planet, Eq. (1) shows that in the limit of zero-A_σ librations the conjunctions of this body with the planet ($\lambda = \lambda_{\rm N}$) happen when $q(-\lambda + \varpi) = \pi$. This means that during conjunctions, the mean anomaly $M = (2k+1)\pi/q$, with k being an integer. For first-order resonances ($q = 1$), the true anomaly v is 180° and the object is in the aphelion of its orbit. Consequently, no encounters with the planet occur even on large-e planet-crossing orbits providing they have sufficiently small A_σ.

The minimum distance between Neptune and the low-amplitude 2 : 3 resonant orbits in Fig. 1b is about 12.2 AU. The distance at aphelic conjunctions is $a(1+e) - a_{\rm N}$, where $a = 39.45$ AU. This gives a distance of 13.3 AU for $e = 0.1$, in good agreement with the minimum distance computed in the simulation, the small difference being related to the fact that the angles initially chosen for the simulation did not permit orbits with $A_\sigma < 60°$ in the 2 : 3 resonance.

In general, at outer resonances of order $q > 1$ the resonant angle σ can librate about one of q distinct centers placed at $(2k+1)\pi/q$, k being an integer. If q is odd, then one of the centers is at 180° and the resonant phase-protection mechanism for zero-A_σ librations about this center works in the same way as for first-order resonances ($q = 1$) assuring conjunctions in aphelia. The other $q-1$ centers are located at $\sigma \neq 180°$ and the zero-A_σ librations about these centers do not have conjunctions at aphelia. If q is even, all centers are at $\sigma \neq 180°$, and again, the conjunctions do not happen at aphelia. The conjunctions condition is $v + \varpi = \lambda_{\rm N}$, and the equation for M at conjunctions can be approximated from $v = M + 2e\cos M + \mathcal{O}(e^2)$, giving

$$M + 2\frac{p+q}{q} e\cos M = -(\sigma_0 + 2k\pi), \qquad (2)$$

where k is an integer and σ_0 is the resonant center under consideration. This equation can be solved for M by iteration, but when the eccentricity is not large, even omission of the first-order term in e gives an acceptable approximation.

In the case of the 3 : 5 MMR at $a = 42.3$ AU, the minimum distance to Neptune in 10^8 yr registered for zero-amplitude librators was 12.6 AU (Fig. 1b). This resonance has two libration centers at $\sigma = 90°$ and 270° and for both of them the conjunctions with Neptune occur at about 90° from perihelia. The distance is $a(1-e^2) - a_{\rm N}$, which for $e = 0.1$ gives 11.7 AU. Equation (2) gives somewhat larger value and still better agreement with the simulation.

In the outer resonances of the type $1:r$, $r \geq 2$, which present asymmetric librations (i.e., $q\sigma_0 \neq 180^\circ$), the phase-protection mechanism is less efficient in separating the orbits from Neptune. For example, in the 1:2 Neptune MMR ($a = 47.8$ AU) with $e > 0.3$ the two centers are placed at about $\pm 68^\circ$ (they vary from $\pm 71^\circ$ for $e = 0.3$ to $\pm 66^\circ$ for $e = 0.4$) so that the conjunctions with the planet can happen relatively close to the perihelion. For $e > 0.37$, where the 1:2 resonant orbits are Neptune-crossing, the potentially stable orbits must necessarily have the maximum excursions of σ less than 65°.

For $e = 0.1$, the two centers of the 1:2 MMR are at $\sigma_0 = \pm 102^\circ$. Assuming that minimum distance happens at conjunction of the two bodies, we compute it by crude approximation of Eq. (2) as $a(1 - e^2)/[1 + e\cos v] - a_N$ with $v = M = 102^\circ$. This gives a minimum distance of 18.2 AU, which is only somewhat larger than the 16 AU determined numerically (Fig. 1b).

2.2. Taxonomy of MMRs

None of the test particles starting with $a > 44$ AU escaped to the Neptune-crossing space (Fig. 1a). Having initially larger a and $e = 0.1$ produced sufficiently large perihelion distances (initially >39.6 AU) that even the nonresonant orbits are well separated from Neptune. Test particles initially placed close to the borders of the 1:2 MMR ($a = 47.8$ and 48.3 AU) had their minimum distances decreased by as much as 5 AU with respect to the background level; this happened because their e increased by more than 0.1 on 10^8 yr. The chaos near borders of the 5:9 and 1:2 MMRs destabilized the orbits that, for $e = 0.1$ and $a > 44$ AU, were found unstable on 4×10^9 yr by Duncan *et al.* (1995). As mentioned earlier, the strength of MMRs is proportional to the eccentricity so that at $e = 0.15$, where Duncan *et al.* (1995) identified additional instabilities between the 4:7 and 1:2 resonances, other MMRs are important (namely 7:13, 8:15, and 9:17).

The LCE estimates (Fig. 1c) show the complex chaotic structure of the transneptunian region. For $a > 44$ AU the plot presents many peaks rising from the background level. We have checked that the main peaks correspond to chaotic regions where the computation of the LCE has converged to a nonzero limit value (see Morbidelli and Nesvorný 1999). The background value of about 10^{-7} yr^{-1} is dictated by the limited integration time span; when the latter is increased, the background level generally decreases. The roughness of the background level in Fig. 1c suggests the general nonintegrability of the motion as discussed for the asteroid belt by Morbidelli and Nesvorný (1999). For $a < 43$ AU, the only orbits with LCE $\sim 10^{-7}$ yr^{-1} are those at centers of the 2:3 and 3:5 MMRs.

The maximum LCE is nonzero in the 7:11 ($10^{-5.6}$ yr^{-1}), 5:8 ($10^{-5.8}$ yr^{-1}), and 8:13 ($10^{-5.8}$ yr^{-1}) MMRs with Neptune, which appear as holes in the more chaotic background in Fig. 1c. Indeed, most orbits placed with the semi-major axes close to these resonances were found unstable over the age of the Solar System by Duncan *et al.* (1995).

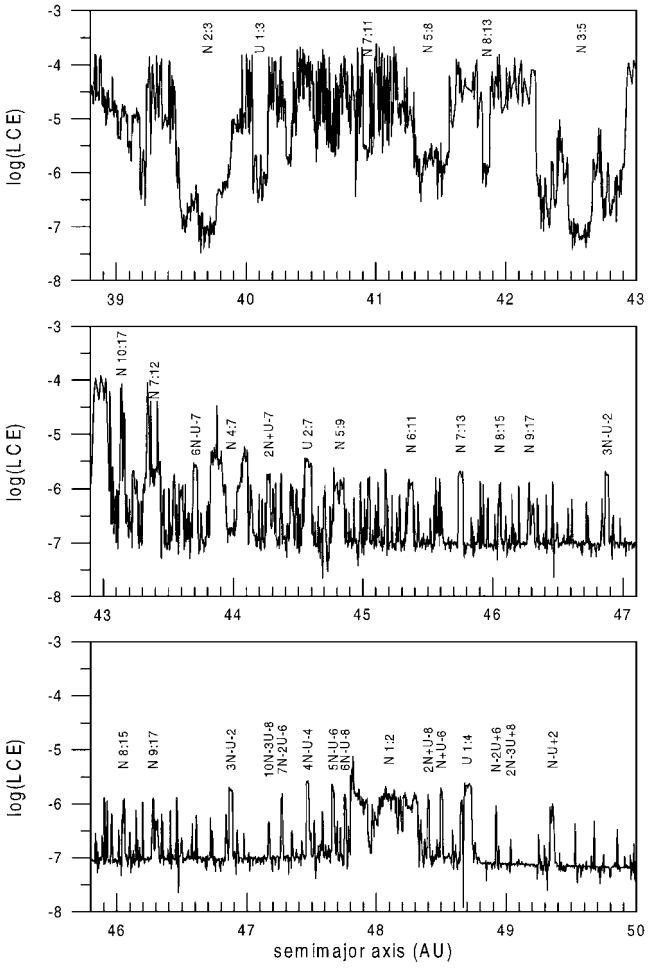

FIG. 2. Enlarged plot of Fig. 1c with the main MMRs being labeled. See text for the notation. Note that the density of resonances increases with decreasing a. Most of the MMRs for $a > 46.5$ AU are the three-body resonances with Neptune and Uranus. The semi-major axis range on the x axis overlaps in the second and third panels.

In analogy to the asteroid belt, most features in the LCE dependence on a observed in Fig. 2 (enlarged from Fig. 1c) are related to MMRs; the secular resonances have lower LCEs due to their longer libration periods. The only exception is the interval 40–42 AU where the three secular resonances (ν_8, ν_{17}, and ν_{18} overlap (Knežević *et al.* 1991), causing escapes in 10^8 yr.

Some of the MMRs are labeled in Fig. 2. These associations[3] were found by short integrations of the test particles having large LCE estimates and by the computation of angles with all resonant combinations that come into question for the given range of semi-major axes. The libration of one resonant angle was usually easily found and the corresponding resonance labeled. The

[3] There is a small shift between the a of the large LCE peaks in Fig. 2 and the mean a of the associated resonances, which is a consequence of short-periodic oscillations in a induced by Jupiter having a 11.8-yr period and a 0.6–0.8 AU amplitude. Consequently, the initial a of a given resonance in our experiment is about 0.25 AU larger than the mean resonant a.

notation in Fig. 2 has the following rules: N$r:s$ is the Neptune resonance with the resonant angle $r\lambda_N - s\lambda + (s-r)\varpi$, where $s > r \geq 1$ are integers; U$r:s$ is the Uranus resonance with the resonant angle $r\lambda_U - s\lambda + (s-r)\varpi$, where λ_U is the mean longitude of Uranus; and the resonances labeled as n_NNn_UUn, with n_N, n_U, and n being integers, are the three-body resonances with the resonant angle $n_N\lambda_N + n_U\lambda_U + n\lambda - (n_N + n_U + n)\varpi$ (Nesvorný and Morbidelli 1998).

While for $a < 46.5$ AU the largest peaks are associated with the MMRs with Neptune, for $a > 46.5$ AU most peaks correspond to the three-body resonances with Neptune and Uranus. We remark that the latter are placed on both sides of the 1 : 2 Neptune MMR according to a peculiar structure, which is a consequence of Uranus and Neptune being close to the mutual 1 : 2 mean-motion resonance: the angle $\lambda_U - 2\lambda_N$ circulates with a negative derivative and a period of about 4230 yr. The sum of a multiple of this angle, $j(\lambda_U - 2\lambda_N)$, j being an integer, with a multiple of the resonant angle of the 1 : 2 Neptune MMR, $k(\lambda_N - 2\lambda)$, k being an integer, gives $(k-2j)\lambda_N + j\lambda_U - 2k\lambda$. This last expression, with appropriate values of k and j, gives the resonant combinations of all 12 labeled MMRs with $a > 46.5$ AU (including the 1 : 4 resonance with Uranus at $a = 48.7$ AU for $k = 2$ and $j = 1$). As the three-body MMRs appear in the perturbation approach at the second order in planetary masses (Nesvorný and Morbidelli 1999), the above observation gives a hint on what combinations of the perturbation harmonics give rise to the identified three-body resonances.

Figure 2 shows that chaotic regions become denser with decreasing a. In fact, the location of MMRs of a given order become denser approaching Neptune, and the sizes of the coefficients of the resonant harmonics increase with decreasing distance from the main perturbing body. This reflects in the number of visible peaks. The height and width of each peak is roughly proportional to the square root of the size of the coefficient of the corresponding resonant harmonic (Murray and Holman 1997, Nesvorný and Morbidelli 1999).

2.3. The Resonant-Driven Evolution of Eccentricity

What are the possible dynamical consequences of the complex resonant structure of the transneptunian region revealed by Fig. 2? In analogy to the asteroid belt, each thin MMR represents a track at a given semi-major axis where the eccentricity and inclination chaotically change on long time periods (Murray and Holman 1997). We give an example of this chaotic evolution in Fig. 3.

The numerical simulation was performed with four outer planets (Jupiter to Neptune) and 101 test particles. The initial positions of planets were taken from JPL DE403 ephemeris for the date 1/1/1998 (JD 2450814.5) with respect to the invariable plane of LONGSTOP 1B simulation (Nobili *et al.* 1989). The initial conditions of test particles were chosen as equidistantly spaced in the interval $37 \leq a \leq 39$ AU ($\Delta a = 0.02$ AU), with $e = 0.01$ and $i = 2^\circ$. The initial angles of test particles were

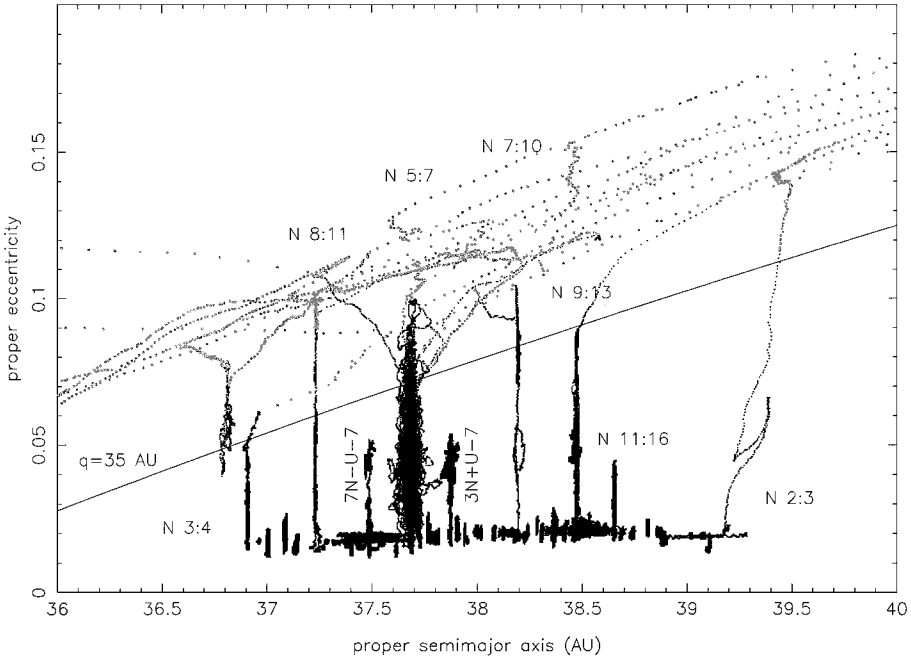

FIG. 3. The chaotic evolution of orbits initially at 37–39 AU with low e and i. The dark points denote the trajectory of a test particle before it first comes to a distance of 2 AU from Neptune's orbit. The large gray symbols show the trajectory after this moment. Sixteen percent of integrated test particles were transferred to Neptune-crossing orbits in 4×10^9 yr. The low-e orbits were modified by slow chaotic diffusion in e driven by labeled MMRs with Neptune (and Uranus). The line of proper $q = 35$ AU is shown for reference. Note that the proper a of all test particles stays almost constant under this line (excluding that at $a > 39$ AU, which started close to the left border of the 2 : 3 MMR). The changes of proper a in the part of the trajectory denoted by gray symbols is due to the effect of close encounters with Neptune.

chosen randomly from a uniform distribution between 0 and 2π. The orbits of planets and test particles were propagated in time using the `swift_rmvs3` integrator (Levison and Duncan 1994) with a 1-yr time step. The total integration time was 4×10^9 yr.

The orbital elements of test particles were averaged over a shifting window of 10 Myr using the same procedure as Morbidelli and Nesvorný (1999, their Eq. (1)). The 10-Myr interval is long enough to cancel out all important quasi-periodic oscillations of orbital elements. Therefore, in the case of local integrability of the equations of motion, the orbital elements defined by the above averaging do not change with time. They are integrals of the motion and are usually called *proper elements*. Conversely, the change of proper elements with time reveals non-quasi-periodic evolution, i.e., *chaotic diffusion*. For purposes of Fig. 3, the proper elements were computed every 10^5 yr.

The dark points in Fig. 3 denote the trajectory before it first became Neptune-grazing (if ever), i.e., before the test particle's osculating perihelion first happened to be close to Neptune's orbit. We choose a threshold distance of 2 AU. Larger gray symbols show the evolution of the trajectory after this instant. The proper perihelion line $q = 35$ AU is shown for reference as an approximate limit above which Neptune dominates the motion. Note however that this is only a rough criterion due to the secular oscillations of osculating eccentricities.

The simulation resulted in 16 escapes to Neptune-crossing orbits. The escapes of two test particles at the extreme left of the integrated a interval happened at the chaotic border of the 3 : 4 Neptune MMR (centered at 36.48 AU). The particle escaping at the extreme right of the integrated interval was initially placed near the chaotic border of the 2 : 3 MMR (centered at 39.45 AU). The remaining 13 particles that became Neptune-crossers during the integration time span evolved from their respective initial locations (initial proper $e < 0.02$) due to a gradual enlargement of the proper e. Such enlargement happened at the positions of second- and higher-order MMRs with Neptune and at locations of three-body resonances with Neptune and Uranus. While the proper a of these particles stayed almost constant at this stage of orbital evolution (dark points), the resonant-driven chaotic diffusion enhanced the objects' proper e; above the line of proper $q = 35$ AU, Neptune close encounters became important. Under the effect of Neptune encounters, these bodies started to random-walk in a, roughly following the curves of invariant Tisserand parameter with respect to Neptune (Valsecchi and Manara 1997). This second stage of orbital evolution was much shorter and the test particles normally reached heliocentric distances larger than 100 AU in a time interval typically not exceeding 10^8 years, at which point they were removed from the simulation. The integration of all 16 particles escaping to Neptune-crossing orbits were stopped before $t = 4 \times 10^9$ yr.

Most of the escaping test particles (9) did so via the 5 : 7 Neptune MMR ($a = 37.68$ AU). In fact, these were all particles that had the initial proper a in the range 37.6–37.75 AU. The size of this interval is about the size of the 5 : 7 MMR determined in the circular planar problem for $e = 0.02$ (=mean initial proper eccentricity of nine escaping particles), which is approximately 0.12 AU. The crossing time (the time elapsed from $t = 0$ to the first crossing of Neptune's orbit) varied between 322 and 1469 Myr with a mean value of 666 Myr. After becoming Neptune grazers, particles were deactivated when some stopping criteria were satisfied (either the heliocentric distance being larger than 100 AU or the test particle being closer than 0.01 Hill radius to any planet), after on average 13 Myr.

Other escapes (one per resonance) occurred at locations of the 8 : 11 ($a = 37.23$ AU, crossing time 641 Myr), 7 : 10 ($a = 38.19$ AU, 620 Myr), and 9 : 13 ($a = 38.47$ AU, 1419 Myr) resonances. The longer crossing time at the 9 : 13 MMR is due to its higher order (4) and smaller chaotic diffusion rate. (See references below). The eccentricity was significantly excited at the 11 : 16 Neptune MMR ($a = 38.654$ AU) and also at the three-body resonances with Neptune and Uranus: $7\mathrm{N} - \mathrm{U} - 7$ (resonant angle, $7\lambda_\mathrm{N} - \lambda_\mathrm{U} - 7\lambda + \varpi$) and $3\mathrm{N} + \mathrm{U} - 7$ ($3\lambda_\mathrm{N} + \lambda_\mathrm{U} - 7\lambda + 3\varpi$). These latter resonances are placed at 37.487 and 37.878 AU, respectively.

The escape mechanisms from the low-e region 37–39 AU shown in Fig. 3 are analogous to those of inner belt asteroids to Mars-crossing orbits (Migliorini *et al.* 1998, Morbidelli and Nesvorný 1999). The analytic estimates of the resonant size, LCE, and diffusion rate at the MMRs in the asteroid belt (Murray and Holman 1997, Murray *et al.* 1998, Nesvorný and Morbidelli 1999) apply also to the KB.

The speed of chaotic evolution at a MMR depends on its strength (Murray and Holman 1997): for some resonances (e.g., on the borders of the 7 : 12 Neptune MMR located at about 43.4 AU) the speed of the chaotic diffusion is enough to enlarge the initial e to the critical value above which the orbit becomes Neptune grazing and the body escapes in 10^8 yr (Fig. 1). There thus must be many test particles escaping from weaker MMRs on longer time intervals. Hence we believe that the thin MMRs are responsible for escapes in many narrow regions in a found by Duncan *et al.* (1995) for $45 < a < 47$ AU. Moreover, this also means that if there were not not enough new bodies injected into the resonances (by collisions or mutual interaction between the KBOs), escaping bodies must open narrow gaps or at least cause local density reductions at the resonant semi-major axes.

For a weak MMR and the resonant body with initially small e, the process of slow chaotic diffusion normally results only in a moderate change of e (and i) over the age of the Solar System. Consequently, this could have caused a chaotic "processing" of KBOs in e (and i) and an alteration of the original characteristics of the KB. By this we mean that the KB is not dynamically "frozen." Whatever structures has been formed in it (collisional families, for example) have dispersed with time and should have depended with other slowly diffusing (in e and i) resonant bodies. The first traces of such a process are being recently revealed on the much better known distribution of asteroids in the main belt (Milani and Nobili 1992, Morbidelli and Nesvorný 1999).

Assuming a uniform distribution of KBOs in the interval $45 < a < 47$ AU and $e = 0.1$, the number of *resonant* objects must be proportional to the total phase space volume occupied by

resonances. In Fig. 2 we can identify about 80 peaks with LCE $> 10^{-6.8}$ yr^{-1} in this interval. These peaks have a total width of about 0.512 AU, which means that about 26% of KBOs at $45 < a < 47$ AU and $e = 0.1$ must be chaotic with LCE $> 10^{-6.8}$ yr^{-1}. Therefore, a significant chaotic evolution in e (and i) may be expected for this part of the KB.

Outside the MMRs (Fig. 3), the proper elements of test particles almost do not change. The small variation of proper a and e for nonresonant orbits validates our calculation of proper elements as 10-Myr averages; these orbits are expected to be close to regular. Note that there is no tendency to alter the proper a, and thus it is practically impossible for the initially nonresonant particles to reach one of the diffusion tracks at resonances.

This result confirms the conclusion of Duncan *et al.* (1995) that under the perturbations of four outer planets most low-e orbits with initial a between the outer edge of the 3 : 4 Neptune MMR (37 AU) and the inner edge of the 2 : 3 MMR (39 AU) are stable over 4×10^9 yr. Because of this orbital stability, one would expect that there exist KBOs with $37 < a < 39$ AU, $q > 35$ AU, and $i < 10^\circ$. Nevertheless, observations have not provided a single object (among 63 known KBOs with good orbits in September 1999) with orbital elements in this interval.[4] Duncan *et al.* (1995) suggested that some mechanism other than the long-term gravitational effects of four outer planets must have cleared it. The effect of Neptune-scattered large planetesimals (Petit *et al.* 1999), sweeping MMRs (Malhotra 1995), or sweeping secular resonances (H. F. Levison *et al.* 1999, preprint) are three different possibilities of how this might have been achieved during the primordial stage of the KB formation.[5]

[4] The recent recovery of 1998 SN165 (Gladman *et al.* 2000b) suggests that this object has the orbital elements $a = 38.1$ AU, $e = 0.05$, and $i = 5^\circ$. This indicates that the concerned region is not completely void of objects and probably hosts a considerable number of KBOs. Still, based on the discovery rate, the region is underpopulated in comparision with other stable places in the KB.

[5] We have also checked another possibility and in this context recall the particular geometry of Pluto's orbit: the argument of Pluto's perihelion oscillates around 90° with an amplitude of 22°. This, together with the equation of ellipse,

$$r = \frac{a(1-e^2)}{1+e\cos v}, \tag{3}$$

where r and v are the heliocentric distance and true anomaly of Pluto, $a = 39.45$ AU and $e = 0.25$, shows that Pluto intersects the ecliptic plane close to $v = \pm 90^\circ$ at a heliocentric distance of about 37 AU. Consequently, the low-e and low-i objects with $a \sim 37$ AU may encounter Pluto when it passes through ecliptic whenever the phasing of orbital revolutions is correct. However, the numerical simulation with five planets (Jupiter to Pluto) showed that Pluto's effect over the age of the Solar System is almost negligible in the interval 37–39 AU, the escape rate being the same as in the simulation with four planets. This is due to the fact that Pluto's inclination (17.2°) and eccentricity (0.25) determine a relatively high velocity at intersection with the orbit at $a = 37$ AU and $e = i = 0$:

$$V = 2\pi\sqrt{2\frac{1-\cos i_P}{a}} = 0.3 \text{ AU/yr} = 1.5 \text{ km/s}, \tag{4}$$

and the deflection of passing trajectories—proportional to V^{-2}—is small. In fact, Pluto gravitational sweeping has a negligible effect on the distribution of objects in the KB (Gladman *et al.* 2000a), with the exception of moderately and high-inclined Plutinos (Nesvorný *et al.* 2000).

3. THE 1 : 2 MMR WITH NEPTUNE

The 1 : 2 resonant angle $\sigma_{1:2} = \lambda_N - 2\lambda + \varpi$ oscillates—unlike in the case of most other MMRs—around a center that is neither 0° nor 180°. Such a case is usually referred to as an *asymmetric* libration, and is found exclusively in the 1 : 1 MMRs (tadpole orbits) and the MMRs exterior to a planet of the type 1 : 2, 1 : 3, 1 : 4, etc. (Beaugé 1994, Morbidelli *et al.* 1995). Consequently, the range of A_σ accessible to stable resonant librations in the 1 : 2 MMR with Neptune is smaller.

In the following experiment, the initial angles of test particles were chosen so that $\sigma_{1:2} = \sigma_0(e)$, $\varpi = \varpi_N$, and $\Omega = \Omega_N$, where $\sigma_0(e)$ is the asymmetric libration center for given e. Figure 4a shows $\sigma_0(e)$ computed by a semi-numerical method in the restricted three-body model with Neptune on a circular and planar orbit. Figure 4b shows an analytically computed maximum possible $A_\sigma(e)$ of tadpole orbits. For A_σ exceeding this value, the motion happens on horseshoe trajectories.

We have run simulations for two sets of initial conditions:

(1) 707 test particles with $47.5 \le a \le 48.5$ AU ($\Delta a = 0.01$ AU), $e = 0.04$, 0.1, 0.2, 0.25, 0.3, 0.35, 0.4 (101 test particles at each e) and $i = 5^\circ$;

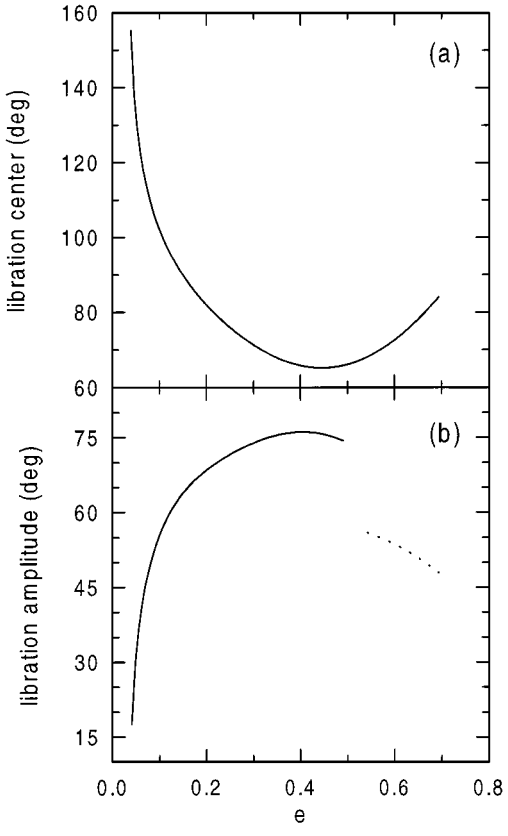

FIG. 4. (a) The asymmetric center (σ_0) of the 1 : 2 MMR as a function of eccentricity. The other center is placed symmetrically in the interval $[-\pi, 0]$. (b) The maximum amplitude of tadpole orbits determined as half-width of the libration island enclosed by separatrices. The discontinuity at $e = 0.5$ is due to the change in the resonant topology introduced by collisions with Neptune. The dashed line approximates the half-width of the tadpole island for $e > 0.5$.

(2) 606 test particles with $a = 47.95$ AU, $0 \le e \le 0.4$ ($\Delta e = 0.004$) and $5 \le i \le 30^\circ$ ($\Delta i = 5^\circ$, 101 test particles at each i).

In the first set we sampled the resonant orbits with small i; the dynamics at larger i was explored in the second set.

As in N&R00, test particles were numerically integrated with four outer planets (Jupiter to Neptune) for 10^8 yr by the symmetric multistep integrator. The initial conditions of the planets were taken from JPL DE403 ephemeris for the date JD 2449700.5 with respect to the mean ecliptic and equinox J2000. The time steps of 40 days for the planets and 200 days for the test particles were used. A smoothing filter was applied to $a \exp \iota\sigma$, $e \exp \iota\varpi$ and $i \exp \iota\Omega$ ($\iota = \sqrt{-1}$). This procedure suppressed periods smaller than 5000 yr. See N&R00 for a more detailed description of the experimental setup.

3.1. Regular and Chaotic Dynamics for Small e

Estimate of the maximum LCE and the minimum distance to Neptune in 10^8 yr are plotted as the set (1) of initial conditions in Fig. 5. The color coding in Fig. 5a is the same as that used in N&R00: test particles escaping within the integration time span are shown in yellow while test particles with smallest LCE are shown in blue. In Fig. 5, we have compensated the scale on the x axis for the short-periodic variations of the semi-major axis with a shift of 0.18 AU in a, so that the test particles with $A_\sigma \sim 0$ are near the true resonant center at 47.8 AU.

In Fig. 5a, we plot the libration centers and separatrices of tadpole orbits (bold vertical line at 47.8 AU and bold lines joining each other at $e = 0.04$ and delimiting the "V"-shaped resonant region). The exterior bold lines are the limits of horseshoe orbits. The Kozai resonance is shown by the thin full line. We have computed its location from $f_\varpi - f_\Omega = 0$, where $f_\varpi(a, e)$ and $f_\Omega(a, e)$ were numerically computed in our experiment. The Kozai resonance intersects the libration center of the 1 : 2 Neptune MMR at $e \sim 0.38$, but we were unable to plot its location at $0.35 < e \le 0.38$, because our initial conditions did not sample this interval.

The dashed line in Fig. 5a shows the 5 : 1 commensurability between the resonant frequency and the frequency of the angle $\lambda_U - 2\lambda_N$. The 4 : 1 commensurability between the same angles is at larger eccentricities and its location at $e = 0.35$ is indicated by two arrows. The 4 : 1 three-body resonance has the same "U"-shaped form as the 5 : 1 resonance and intersects the libration centers of the 1 : 2 Neptune MMR at $e \sim 0.32$.

From 191 KBOs currently registered in the Asteroid Orbital Elements Database of the Lowell Observatory (ftp://ftp.lowell.edu/pub/elgb/astorb.html), six objects are close to the 1 : 2 Neptune MMR ($46.5 < a < 49$ AU). Computing the smoothed orbital elements (i.e., the orbital elements from which the short periodic variations has been removed—see N&R00) of these objects, we find that only one object—1997 SZ10—falls within the interval of a and e shown in Fig. 5. A pair of two-headed vertical arrows has been placed in this figure, indicating the extrema of filtered a and e of 1997 SZ10 (determined from a numerical integration of its orbit over 10^7 yr). This figure indicates that this object is on a horseshoe orbit with $A_\sigma \sim 150^\circ$, which is unstable on 10^8 yr. However, there is a large uncertainty in the semi-major axes of this and the other five bodies that were computed from small observational arcs, so that conclusions would be premature. In contrast, we believe from the following reasons that two of the above six objects are on stable resonant orbits.

Our argument is based on the orbital angles of 1997 SZ10 and 1996 TR66, which according to E. Bowell (personal communication) are quite determinate,[6] conversely to the semi-major axes, which have 1-σ uncertainties of $\sim$0.07 and $\sim$0.31 AU, respectively. It is interesting to note that the present value of $\sigma_{1:2}$ of 1997 SZ10 (at JD 2449700.5) is -69°, which is almost exactly the value of the second resonant center $\sigma_0(e) \sim -67^\circ$ at $e = 0.36$ (Fig. 4a). This coincidence is quite surprising because the orbital angles were not deliberately chosen to put 1997 SZ10 close to the libration center. This shows that it is quite possible that this object is in fact a stable resonant body with the semi-major axis erroneously (by some 0.2–0.3 AU) determined from observations. Moreover, the second object—1996 TR66—which falls close to the 1 : 2 Neptune MMR has $\sigma_{1:2} = -62^\circ$, again very close to the corresponding $\sigma_0(e)$ for $e \sim 0.38$.[7] This should not be a mere coincidence because the probability that $\sigma_{1:2}$ of a discovered object is within 5° from to one of the libration centers (as it happens for both 1997 SZ10 and 1996 TR66) is 1 in 18. Indeed, for nonresonant objects, $\sigma_{1:2}$ circulates and receives values between 0° and 360° with equal probability. Consequently, at the time of observation, the nonresonant bodies would be uniformly spread in $\sigma_{1:2}$ between 0° and 360°.

As we will show in Section 3.3, the stable resonant objects with $e \sim 0.3$ are expected to move within $\pm 30^\circ$ from $\sigma_0(e = 0.3)$. At $e \sim 0.36$–0.38, where the limit of the stable tadpole motion is smaller than at $e = 0.3$ (Fig. 5), the stable resonant objects must always stay closer than 10°–20° to σ_0, exactly at a place where 1997 SZ10 and 1996 TR66 are currently located. Moreover, if both objects are resonant bodies, they probably also fall into the Kozai resonance since, at present, $\omega = 341^\circ$ for 1997 SZ10 and $\omega = 311^\circ$ for 1996 TR66, and for $e = 0.38$ the stable ω libration happens around $\omega_0 = 325^\circ$ (Section 3.4).

On the other hand, we still cannot exclude the possibility that 1997 SZ10 and 1996 TR66 are captured scattered disk objects

[6] The assumed orbital elements of 1997 SZ10 and 1996 TR66 on 8/10/1999 (JD 2451400.5) are $a = 48.6752$ AU, $e = 0.37419$, $i = 11.768^\circ$, $M = 11.393^\circ$, $\omega = 341.122^\circ$, $\Omega = 9.422^\circ$, and $a = 47.3227$ AU, $e = 0.38081$, $i = 12.3906^\circ$, $M = 35.732^\circ$, $\omega = 311.325^\circ$, $\Omega = 342.993^\circ$, respectively. Note also that B. Marsden give similar solutions for the orbital angles of 1997 SZ10 and 1996 TR66.

[7] The uncertainty domains of the orbital elements are such that the true semi-major axes of 1997 SZ10 and 1996 TR66 may be as far as 0.4 and 2 AU from their current nominal orbits, respectively, without significantly alternating their orbital angles (J. Virtanen and K. Muinonen, personal communication).

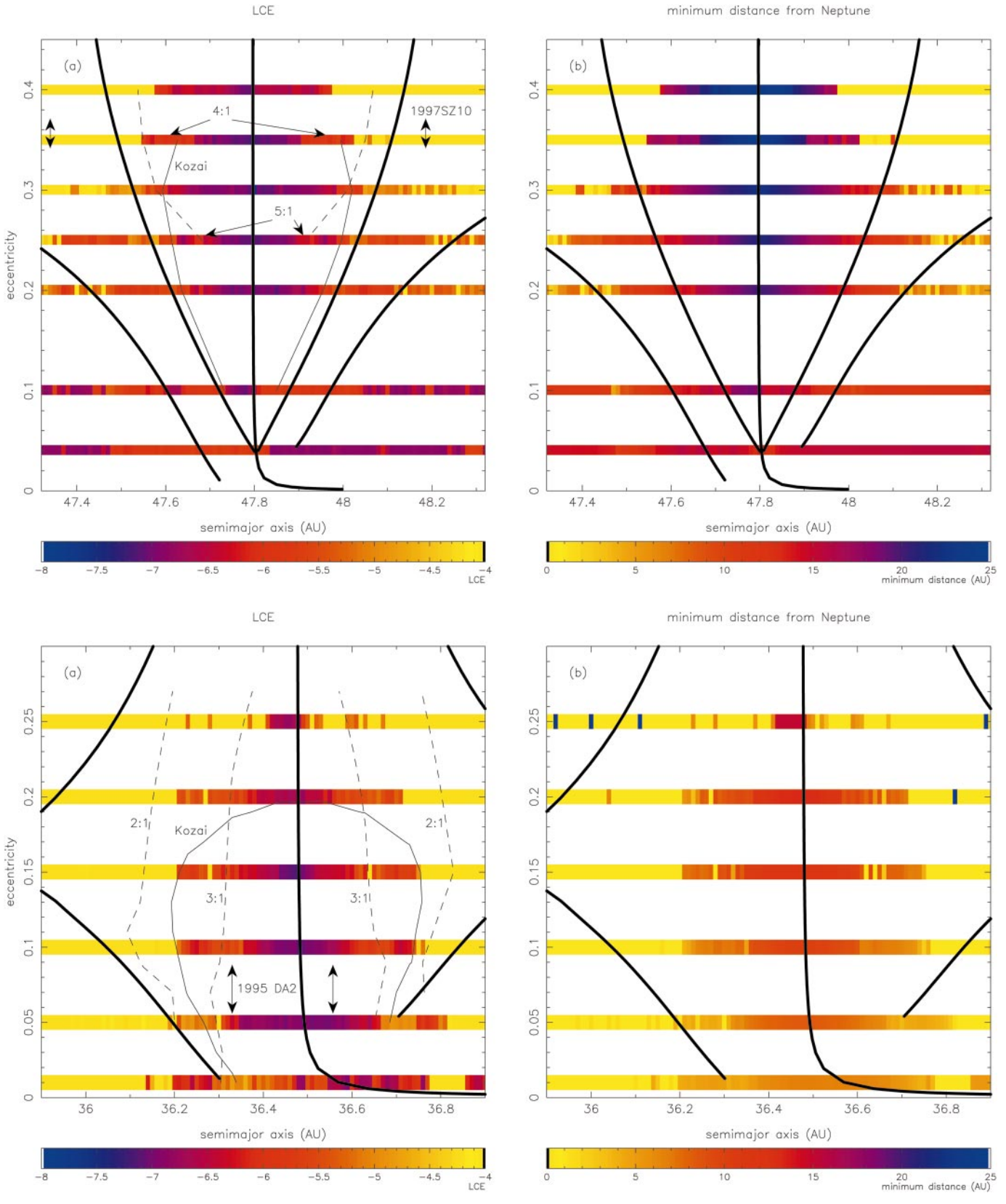
LCE
minimum distance from Neptune
(a)
(b)
4:1
1997SZ10
Kozai
5:1
eccentricity
semimajor axis (AU)
LCE
minimum distance (AU)
2:1
3:1
1995 DA2

(Duncan and Levison 1997). Such bodies spend about 20% of their lifetimes within 5° from σ_0 (H. Levison, personal communication). So, the probability of seeing captured objects where 1997 SZ10 and 1996 TR66 are currently located is small but not completely negligible.

In Fig. 5a, the LCE is smaller than $\sim 10^{-7}$ yr^{-1} in the central region of the 1 : 2 MMR, which shows orbital regularity comparable to that of the central region of the 2 : 3 MMR (N&R00, their Fig. 2). The central region is the widest for $e = 0.3$, where it accounts for almost 0.4 AU in a. This is much less than the resonant size computed by Malhotra (1996) for the same e in the circular and planar model with Neptune. Our computation shows that the central region of the 1 : 2 MMR at $e = 0.3$ is similar in size to the stable region of the 2 : 3 MMR.

For smaller and larger e, the region of small LCE of the 1 : 2 MMR shrinks. There is a large gradient of the period of σ with respect to e so that at $e = 0.1$, the libration frequency is comparable to the perihelion and node frequencies. For $e < \sim 0.1$, the tadpole region is very narrow and the $A_\sigma \sim 0$ tadpole orbits are destabilized on short time scales. These orbits later evolve alternating between circulation and horseshoe regimes, with short intermittences of tadpole librations. The resonant motion at $e \sim 0.4$ and small A_σ is moderately chaotic (LCE $\sim 10^{-6.5}$ yr^{-1}). This is not because of the effect of Neptune encounters (Fig. 5b) but rather an influence of the Kozai resonance. In Section 3.4, we show by long-term numerical simulation that the resonant motion is unstable over 4×10^9 yr when $e > \sim 0.4$.

One can also note in Fig. 5a that the chaos is enhanced at the 4 : 1 and 5 : 1 three-body resonances, where LCE $\sim 10^{-5.8}$ and $\sim 10^{-6.2}$ yr^{-1}, respectively. These values are similar to those found at the same three-body resonances in the 2 : 3 Neptune MMR (N&R00, their Fig. 2a). Here however, the resonant positions are quite different (4 : 1 resonance is "inner" to 5 : 1 resonance), with a shape following convex lines (5 : 1 is shown by dashed line in Fig. 5a). This particular configuration is related to the fact that inside the asymmetric island of the 1 : 2 MMR, the libration period increases when approaching the separatrices while at the 2 : 3 MMR, the libration period decreases when approaching to the separatrices.

The horseshoe orbits in the 1 : 2 MMR are generally chaotic ($\ln \Delta(t)/t = 10^{-5}$–$10^{-6}$ yr^{-1} with $t = 10^8$ yr). Although we have not investigated the sources of this chaos in detail, one reason could be the large period of σ for horseshoe orbits (roughly double of the period for tadpole orbits for the same e). Thomas and Ferraz-Mello (2000, in preparation) have shown that the secondary and secular resonances are frequently present in the horseshoe regime of the 1 : 1 MMR with a planet.

Figure 6 shows the measures of chaotic evolution of the orbital elements, δA_σ (a), δe (b), and δi (c), and of frequencies, δf_σ (d), δf_ϖ (e), and δf_Ω (f). These quantities have been determined in the same way as in N&R00 (their Eqs. (2)–(4)). δA_σ, δe, and δi are the chaotic changes of orbital elements over 45 Myr. δf_σ, δf_ϖ, and δf_Ω are the relative changes of frequencies over the same time interval.

Comparing Figs. 5 and 6, one can see the correlation between the values of the LCE and the measures of chaotic evolution of orbital elements. For example, the orbits are very stable in the core of the 1 : 2 MMR where the LCE is small. Figure 6 is nevertheless more rigorous concerning the orbital stability/instability, specifically:

(1) The most stable place in the 1 : 2 MMR is at $e = 0.3$, where $\delta A_\sigma = 0.1°$ per 45 Myr for $A_\sigma < 30°$ (Fig. 6a). There the expected change of A_σ over 4.5 Byr is 1°. Even if $e = 0.3$, the maximum A_σ available for tadpole orbits is 70° (Fig. 4b), for $A_\sigma > 30°$, such orbits are already unstable and escape from the resonance.

(2) Stable tadpole motion practically does not exist for $e < 0.1$ and for $e > 0.4$, where $\delta A_\sigma > 1°$ per 45 Myr. While in the former case, the test particles may still survive several billion years on horseshoe orbits, because their e is small, in the latter case, the test particles are efficiently removed from the resonance by encounters with Neptune.

(3) The chaotic structure of the resonant region at intermediate eccentricities ($0.1 < e < 0.4$) is complex. Apart from the resonances shown in Fig. 5a, there are the $2(g - s_8) = 0$ secular resonance at $e \sim 0.2$ and the $2g - s - s_8 = 0$ secular resonance at $e \sim 0.3$, for $A_\sigma \sim 0$ (g and s are the perihelion and nodal frequencies of test particle, and $g_8 = 0.673$ arcsec yr^{-1} and $s_8 = -0.691$ arcsec yr^{-1} are the perihelion and nodal frequencies of Neptune).

(4) The horseshoe orbits for $e > \sim 0.3$ are generally unstable on 10^8 yr (yellow in Figs. 5a and 6a–6c). Also for $e < 0.3$, the chaotic evolution of horseshoe orbits is large (Figs. 6a–6c) and many objects are expected to escape from the resonance by increasing their orbital e.

FIG. 5. The maximum LCE (a) and minimum distance to Neptune (b) computed for $i = 5°$ and several a, e in the 1 : 2 MMR with Neptune (set (1) of initial conditions). The x-axis scale was corrected for the difference between initial osculating and mean resonant semi-major axis due to short-period perturbations. The resonant center and the limits of tadpole and horseshoe orbits are shown by bold lines. Inner resonances are denoted by thin lines (the location of the 4 : 1 three-body resonance is indicated only for $e = 0.35$). The current orbital elements of 1997 SZ10 would indicate a horseshoe orbit unstable on 10^8 yr (the two-headed vertical arrows delimit the maximum and minimum values of its a and e on 10^7 yr, but see the discussion in text). In the central resonant space, LCE $< 10^{-7}$ yr^{-1}. The minimum distance to Neptune is larger than 20 AU for $A_\sigma \sim 0$ and $e > 0.25$.

FIG. 12. The maximum LCE (a) and minimum distance to Neptune (b) computed for $i = 5°$ and several a, e in the 3 : 4 MMR with Neptune (set (1) of initial conditions). The x-axis scale was corrected for the difference between initial osculating and mean-resonant semi-major axis due to short-period perturbations. The resonant centers and separatrices are shown by bold lines. Inner resonances are denoted by thin lines. The KBO 1995 DA2 has a stable orbit (the two-headed vertical arrows delimit the maximum and minimum values of its filtered a and e on 10^7 yr). In the central resonant space, LCE $< 10^{-7}$ yr^{-1} and the minimum distance to Neptune does not exceed 15 AU and is less than 10 AU for $e < 0.1$.

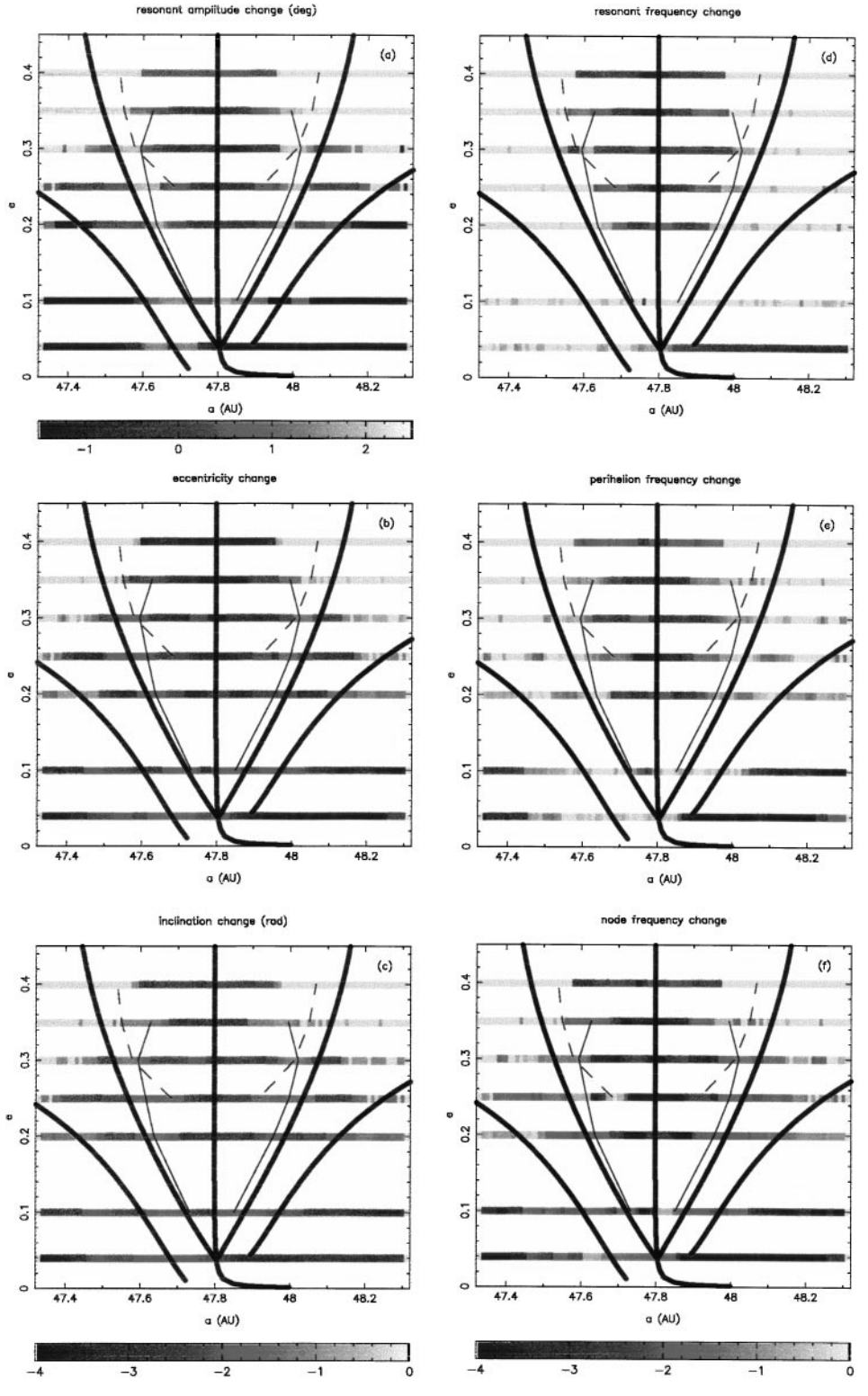

FIG. 6. The changes of orbital elements, δA_σ (a), δe (b), and δi (c), and of the frequencies, δf_σ (d), δf_{ϖ} (e), and δf_Ω (f), measured per 45 Myr, for the set (1) of initial conditions in the 1 : 2 Neptune MMR. The color coding is the same in all panels but (a). The low-A_σ tadpole orbits are stable over the age of the Solar System because the chaotic evolution of orbital elements/frequencies is small there. Apart from the resonances shown in these figures, there are the $2(g - s_8)$ and $2g - s - s_8$ secular resonances located at $e \sim 0.2$ and ~ 0.3 near $A_\sigma \sim 0$, respectively. The horseshoe orbits are generally unstable with ejection times indirectly proportional to the initial e.

3.2. *The Dynamics at $A_\sigma \sim 0$ and Larger i*

The set (2) of initial conditions was designed to study the orbital dynamics near the libration centers. Indeed, the test particles with $a = 47.95$ AU had initially $A_\sigma < 20^\circ$ for $e > 0.1$ (this lower e limit depends on i). For $e < 0.1$, where the tadpole orbits practically do not exist, the studied orbits move in a horseshoe regime. Figure 7a shows the maximum LCE. Figure 7b shows the minimum distance from Neptune over 10^8 years for $i = 10^\circ$.

The particles on the left side of the full thick line in Fig. 7a are chaotic with LCE $\sim 10^{-5.5}$–$10^{-6.5}$ yr^{-1}. The full thick line was empirically traced through LCE $= 10^{-6.5}$ yr^{-1}. On the right side of this line, $\log(\ln \Delta(t)/t)$ almost linearly decreases with $\log t$ and the minimum value of the LCE in Fig. 7a ($\sim 10^{-7}$ yr^{-1}) is dictated by the integration time span. There is only one well-determined structure visible in the plot: for $e > 0.36$ and $i > 15^\circ$, $\ln \Delta(t)/t$ converges to $\sim 10^{-6.5}$ yr^{-1}, where the Kozai resonance is located. The minimum distance from Neptune smoothly decreases with e in the regular region and drops to 15 AU in the chaotic low-e region (Fig. 7b).

Measures of chaotic diffusion (Fig. 8) reveal two secular resonances in the "regular" region. The $2(g - s_8)$ secular resonance is at $e = 0.185$ and the $2g - s - s_8$ resonance is at $e \sim 0.3$. The full thin lines in Fig. 8 were plotted at $2(f_\varpi - s_8) = 0$ (denoted by $2(g - s8)$) and $2f_\varpi - f_\Omega - s_8 = 0$ (denoted by $2g - s - s8$), respectively, where $f_\varpi(e, i)$ and $f_\Omega(e, i)$ were determined numerically in our experiment. The dashed lines were empirically traced at approximate positions of separatrices of the $2g - s - s_8$ secular resonance. This resonance overlaps with the Kozai resonance for $i > \sim 20^\circ$. The resonant angles, $2(\varpi - \Omega_N)$ of the former and $2\varpi - \Omega - \Omega_N$ of the latter, clearly librate for test particles in these resonances. Figure 9 shows the time evolution of $2\varpi - \Omega - \Omega_N$ (9a) and of e (9b) for the test particle with initial conditions: $a = 47.95$ AU, $e = 0.304$ and $i = 10^\circ$. The evolutions are correlated as it is expected for pendulum-like coupled motion of the action and resonant angle.

The total variations of e and i in the "chaotic" region, extrapolated to 4.5 Byr, are 0.2° and 10°, respectively. This suggests a prevailing stability of primordial bodies since the motion in horseshoe regime gets strongly unstable only for $e > 0.3$. The "regular" region at small A_σ is generally stable for $e < 0.35$ and $i < 25^\circ$. The secular resonances may potentially destabilize only the orbits with $i > 25^\circ$. This instability limit of i is about the same as found by Duncan *et al.* (1995) for other resonances.

3.3. *A Simple Model of Chaotic Diffusion*

A one-dimensional random-walk model of chaotic diffusion in the 2 : 3 Neptune MMR was described in N&R00 (see their Section 4 for details). Here, we use the same model for the 1 : 2 MMR.

For a given initial value of A_σ, 1000 test particles were simulated with $e = 0.3$ and $i = 5^\circ$. Assuming a random walk in A_σ, we advanced the orbits of these test particles by applying random kicks of the size of δA_σ (taken from Fig. 6a) to their

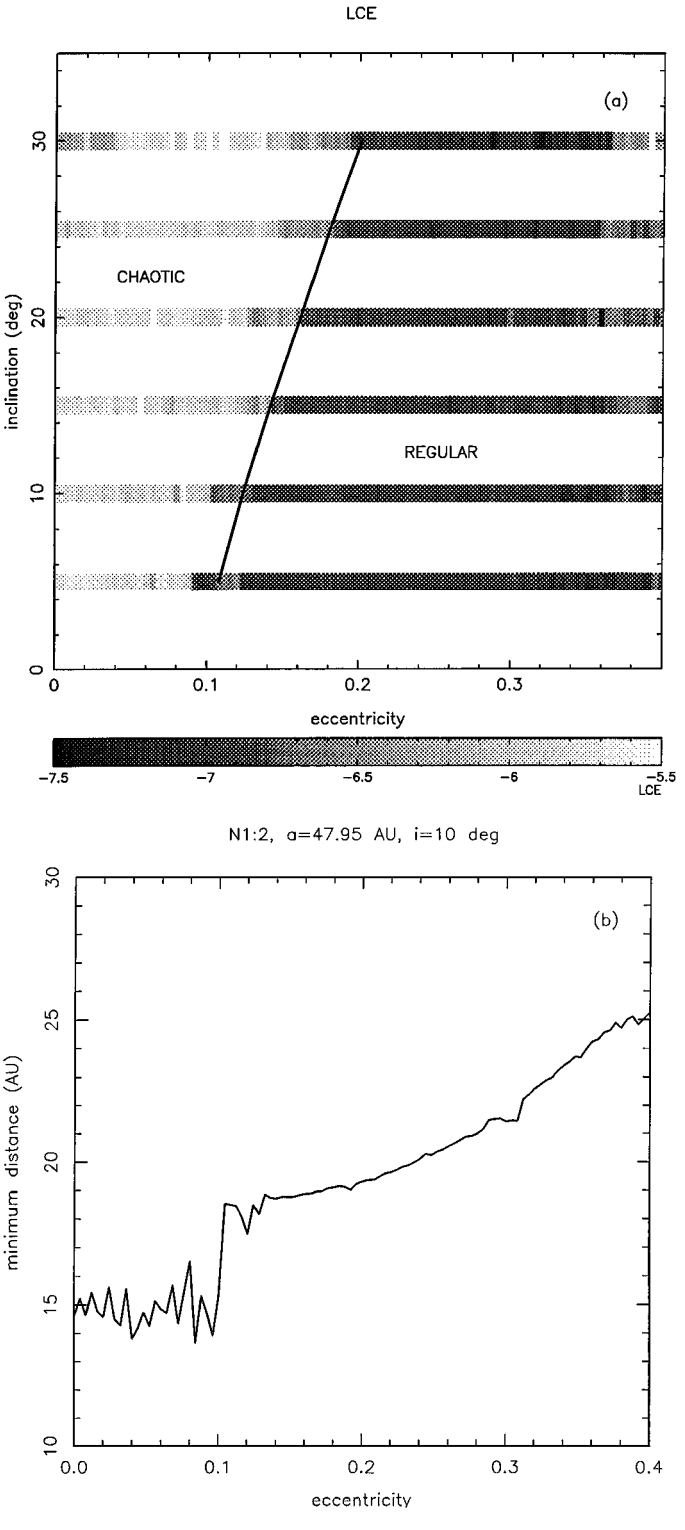

FIG. 7. The maximum LCE (a) and the minimum distance to Neptune (b) for the set (2) of initial conditions in the 1 : 2 Neptune MMR (initial $a =$ 47.95 AU). The bold line in (a) schematically separates two regions with different strengths of chaos. For test particles in the large-e region (denoted by "regular"), $\ln \Delta(t)/t$ does not converge to a limit value on the integration time span. Conversely, in the low–e region (denoted by "chaotic"), LCE $> 10^{-6}$ yr^{-1}.

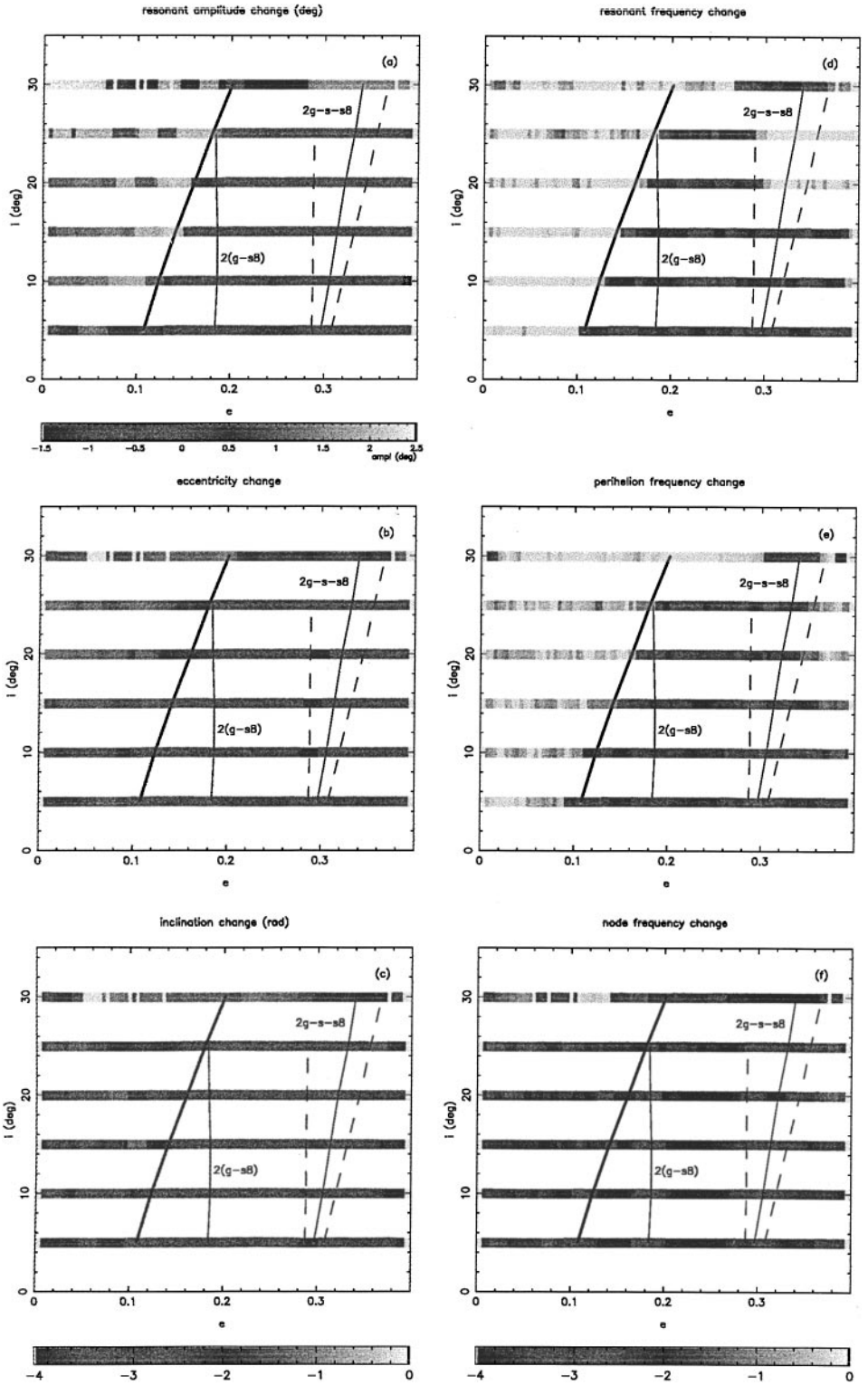

FIG. 8. The changes of orbital elements, δA_σ (a), δe (b), and δi (c), and of frequencies, δf_σ (d), δf_{ϖ} (e), and δf_Ω (f), measured per 45 Myr, for the set (2) of initial conditions in the 1 : 2 Neptune MMR (initial $a = 47.95$ AU). The color coding is the same for all panels but (a). The $2(g - s_8)$ secular resonance is shown by the thin line at $e = 0.185$. The center (full thin line) and approximate positions of the separatrices (dashed thin lines) of the $2g - s - s_8$ secular resonance are shown near $e = 0.3$. The Kozai resonance is at $e \sim 0.38$ and overlaps with $2g - s - s_8$ for $i > 20^\circ$.

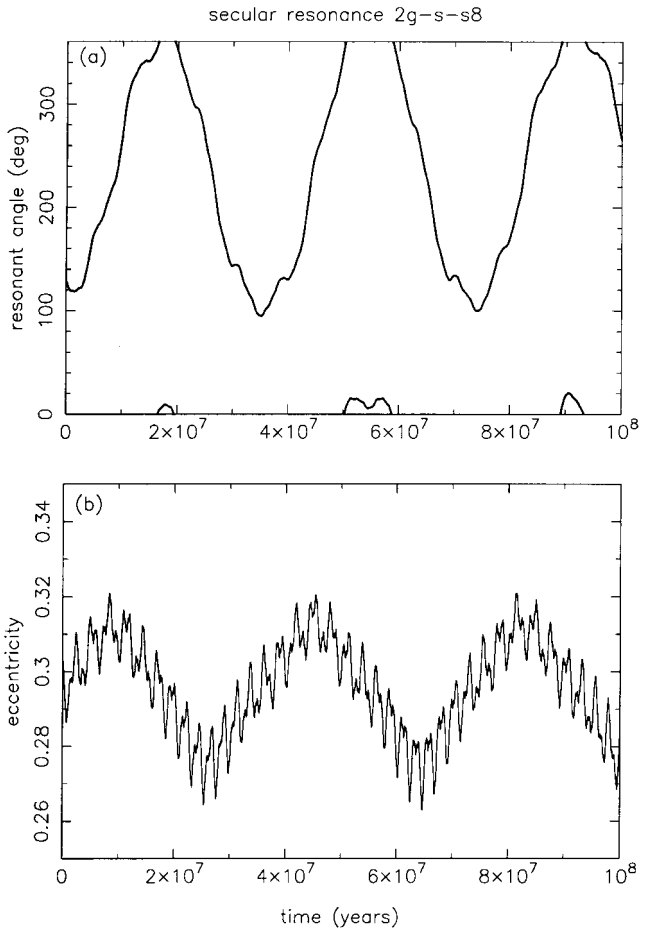

FIG. 9. The evolution of $2\varpi - \Omega - \Omega_N$ (a) and e (b) for a test particle starting with $a = 47.95$ AU, $e = 0.304$, and $i = 10°$. Note that the libration of the angle with a period of ∼40 Myr is correlated with oscillations of e. This particle is in the $2g - s - s_8$ secular resonance.

A_σ. A test particle was deactivated if $A_\sigma > 85°$. This simulation was repeated for 51 different values of A_σ regularly spaced between 0 and 50°. The total volume $V(50°)$ occupied by these orbits is 36.1 AU × deg. The number of surviving test particles was then rescaled to a total number of 1000 particles initially placed in the interval $0 \le A_\sigma \le 50°$, and uniformly distributed in a, λ, ϖ, and Ω.

Figure 10 shows the initial density profile of test particles (dashed line) and the eroded density profile at $t = 4$ Byr (bold line denoted by "+0"). Sixty-four percent of the test particles survived 4 Byr. Most of the escapes happened for $A_\sigma > 30°$, and for $A_\sigma > 50°$ more than 90% of test particles left the resonance. According to Fig. 10, and assuming that only the dynamical diffusion was acting on resonant bodies, the maximum density of the current resonant population should be at $A_\sigma \sim 30°$.[8]

[8] We show in Fig. 10 the distribution of surviving particles vs the *initial* A_σ, which is not much different from the distribution of surviving particles vs the *final* A_σ. The density is still peaked at $A_\sigma \sim 30°$ and decreases somewhat more steeply to larger A_σ than is shown in Fig. 10.

The following qualification is in order. We have assumed in the model that the resonant population was initially uniform in the semi-major axis and angles. This implies that the number of initial objects at A_σ was proportional to the volume in the phase space occupied by orbits with A_σ (see N&R00, Section 4). The initial density has an increasing trend with A_σ (dashed line in Fig. 10), simply because the resonant orbits with larger A_σ occupy larger volume in the phase space and are more frequently sampled. It is generally believed that the model of sweeping resonances and the resonant capture in MMRs in the primordial KB (Malhotra 1995) should have produced a nonuniform distribution in A_σ of the initial population of the 1 : 2 MMR. As discussed in N&R00, this is not a result of the process of resonant capture, but mainly a consequence of the smaller volume of small-A_σ orbits and the dynamical instability at larger A_σ. This is the reason why Malhotra's captured population is peaked at moderate amplitudes. In general terms, we would expect that if the capture simulation carried out by Malhotra (1997) for the 2 : 3 MMR were repeated also for the 1 : 2 MMR, the maximum resonant density of captured KBOs would be at slightly larger A_σ than that in our Fig. 10 (for $e = 0.3$) because of the short time span used in Malhotra's capture simulations for which orbits at large A_σ are still stable. For this reason, our assumption of

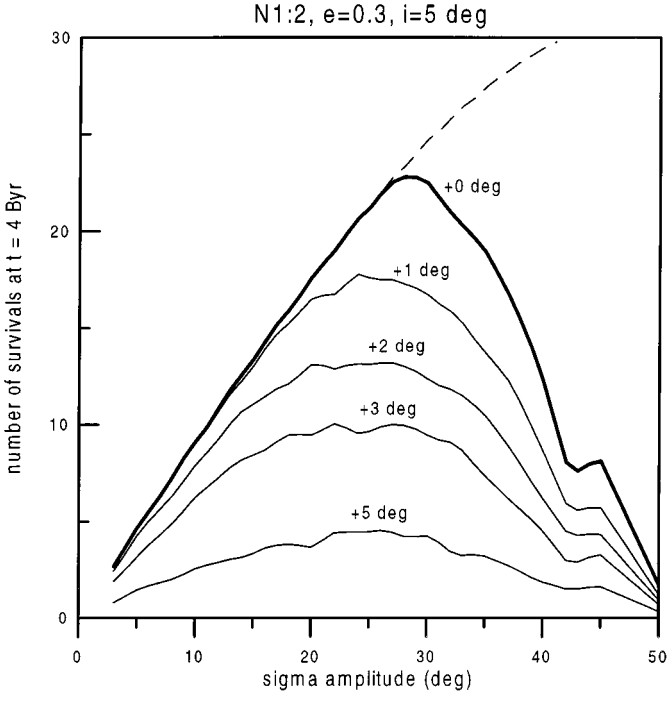

FIG. 10. The number of surviving particles at $t = 4$ Byr in the 1 : 2 MMR ($e = 0.3$ and $i = 5°$) vs initial A_σ. Dashed line shows the initial density distribution in number of particles per 1°. The other lines show the eroded density distributions assuming a random walk at $0 < t < 4$ Byr with a local rate given by $\delta A_\sigma + \delta A_\sigma^{\rm kick}$ (see text). The value of δA_σ is shown in Fig. 6a. The bold line denoted "+0 deg" corresponds to $\delta A_\sigma^{\rm kick} = 0$. The thin lines correspond to values of $\delta A_\sigma^{\rm kick}$ ranging between 1° per 45 Myr (denoted "+1 deg") and 5° per 45 Myr (denoted "+5 deg").

initially uniform semi-major axes and angles is approximately valid for the resonance sweeping scenario.

The other curves in Fig. 10 show the results of additional experiments adding to δA_σ (which is the chaotic diffusion induced by gravitational perturbations of four major planets only), the evolution of A_σ due to random kicks produced by mutual collisions or dynamical scattering: $\delta A_\sigma^{\rm kick} = 1^\circ$ per 45 Myr (53% particles survived), 2° per 45 Myr (41%), 3° per 45 Myr (31%), and 5° per 45 Myr (13%) (see Section 4 in N&R00). The last value shows that $\delta A_\sigma^{\rm kick} > 5^\circ$ per 45 Myr is needed in order to reduce the original population to 1/10.

Of course, this is a very rough model of the real collision dynamics in the 1 : 2 MMR because it does not account for the disruption of bodies and for the resulting changes in the size distribution. In such a case, the loss of resonant KBOs of a given size may have been partially compensated from disrupted larger bodies.

Assuming that the dependence of the primordial KBO density on heliocentric distance r was proportional to $\sim r^{-2}$ (Tremaine 1990) and that the primordial excitation in the 2 : 3 and 1 : 2 MMRs efficiently randomized orbital eccentricities in the interval $0 < e < 0.35$, the ratio between current populations of the most stable places in the resonances ($e = 0.2$ in 2 : 3 and $e = 0.3$ in 1 : 2) is

$$\frac{1}{2}\frac{V(A^*_{2:3})}{V(A^*_{1:2})}\frac{P^{2:3}_{\rm surv}}{P^{1:2}_{\rm surv}}\left(\frac{a_{1:2}}{a_{2:3}}\right)^2, \qquad (5)$$

where $V(A^*_{2:3}) = V(127^\circ) = 116.6$ AU × deg (N&R00), $V(A^*_{1:2}) = V(50^\circ) = 36.1$ AU × deg, $P^{2:3}_{\rm surv} = 0.81$, $P^{1:2}_{\rm surv} = 0.64$, $a_{2:3} = 39.5$ AU, and $a_{1:2} = 47.8$ AU. $P_{\rm surv} = N_{\rm surv}/N_{\rm prim}$ is the relative fraction of objects surviving at $t = 4$ Byr with respect to the number of primordial objects. The factor 2 in the denominator is a result of two asymmetric libration centers in the 1 : 2 MMR against one center in the 2 : 3 MMR.

Evaluating Eq. (5) indicates that there should currently exist three times more objects with $e = 0.2$ in the 2 : 3 MMR than with $e = 0.3$ in the 1 : 2 MMR. The same calculation with survival percentages $P^{2:3}_{\rm surv}$ and $P^{1:2}_{\rm surv}$ evaluated in the experiments with $\delta A_\sigma^{\rm kick} = 3^\circ$ per 45 Myr results in the ratio of 4.25.

There are ∼15 KBOs and Pluto observed at present on stable orbits in the 2 : 3 MMR (N&R00) and two likely candidates for the 1 : 2 MMR resonant bodies (1997 SZ10 and 1996 TR66—Section 3.1). The apparent observational ratio between the 2 : 3 and 1 : 2 MMR populations is thus 8. As the selection observational effect probably contributes by a factor of 0.3 (Jewitt *et al.* 1998), the intrinsic (real) ratio between these two populations should be about 2.5, in a reasonable agreement with the ratio predicted by Eq. (5) with $\delta A_\sigma^{\rm kick} = 0$.

3.4. A Long-Term Simulation of the 1 : 2 Resonant Orbits

In order to verify the long-term stability of orbits in the central region of the 1 : 2 MMR we simulated 40 test particles with initially small A_σ over 4 Byr. We used the `swift_rmvs3` integrator (Levison and Duncan 1994) with a time step of 0.8 yr and included the perturbations of four major planets. The planetary initial conditions were taken from the JPL DE403 ephemeris at JD 2450814.5, with respect to the invariable plane of the LONGSTOP 1B simulation. The initial conditions of test particles were $a = 47.5$ AU, $i = 2^\circ$, and e ranging from 0.04 to 0.45 ($\Delta e \simeq 0.01$). We set initially $\varpi - \varpi_{\rm N} = 0$, $\Omega - \Omega_{\rm N} = 0$, and chose the value of the initial mean anomaly in order to have $\sigma_{1:2} = \sigma_0(e)$, where σ_0 stands for the asymmetric center located between 0° and 180° for the corresponding e (Fig. 4a). This choice of initial conditions implies that all particles with $e > 0.13$ have $A_\sigma < 30^\circ$.

Most simulated orbits with small A_σ survived over the age of the Solar System without any significant change of their mean (A_σ, e, i). The only particles with initially small A_σ that escaped during the simulation were those initially located at $e > 0.41$. At these eccentricities, the overlap of inner resonances (as the 4 : 1 three-body and Kozai resonances) generates a strong chaos, driving particles to the Neptune-crossing orbits.

For $0.37 < e < 0.40$, orbits are affected by the Kozai resonance. In contrast with the classical Kozai resonance, the ω librations do not occur around 90° or 270°, but rather around $\sim 140^\circ$ or $\sim 320^\circ$ (Fig. 11). This is a consequence of the asymmetric libration of $\sigma_{1:2}$. For $0.37 < e < 0.40$, σ librates around $\sigma_0 \sim 65^\circ$.

The shift of the equilibrium points of the Kozai resonance in the 1 : 2 resonance can be explained on the basis of a simple model. Consider the Hamiltonian $\mathcal{H}_{\rm res}$ of the averaged restricted three-body problem, with the massive body on a circular and

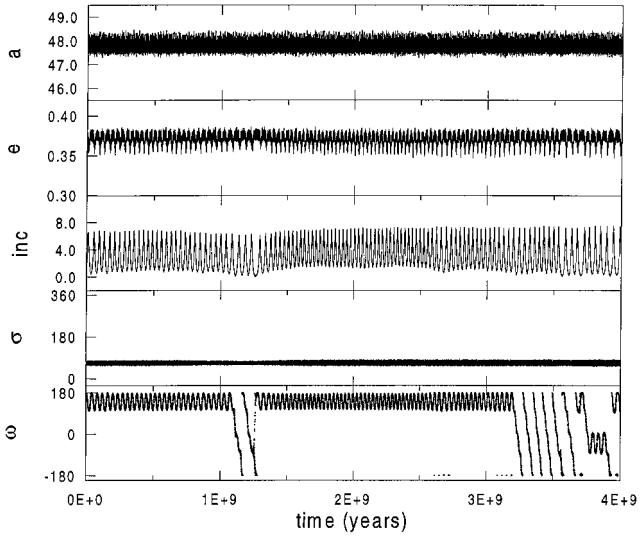

FIG. 11. Evolution of a test particle in the 1 : 2 Neptune MMR. The initial conditions (initial $e = 0.3778$) were chosen so that the orbit of this particle is characterized by small-A_σ libration around $\sigma_0 = 65^\circ$. This particle evolves in the Kozai resonance with ω libration around $\sim 140^\circ$. This libration is correlated with coupled oscillations of e and i.

planar orbit. Expanding its Keplerian part around the resonant semi-major axis a_0, and the perturbing function up to the second degree in inclination, we can write

$$\mathcal{H}_{\rm res} = -\frac{3}{2L_0^2}L^2 - m_1 \times \left[R_0 + \frac{\eta^2}{2}\left(R_1 + R_2\cos 2\sigma_z + R_3 \sin 2\sigma_z\right)\right], \quad (6)$$

where m_1 is the mass of the perturbing body, $L_0 = \sqrt{a_0}$, $L \propto S_z$, $\eta = \sin i/2 \propto \sqrt{S_z}$, and S_z is the action conjugated to $\sigma_z = \sigma + \omega$. The coefficients R_i are functions of a, e, σ and we evaluate them at the MMR's libration center: $R_i = R_i(a_0, e_0, \sigma_0)$ (Roig *et al.* 1998).

This one degree of freedom Hamiltonian can be written as

$$\mathcal{H}_{\rm res} = -\left(\frac{3}{2L_0^2}L^2 + m_1\frac{\eta^2}{2}R_1\right) + m_1\frac{\eta^2}{2}R\cos(2\sigma_z + 2\phi), \quad (7)$$

with

$$R = \pm\sqrt{R_2^2 + R_3^2} \quad (8)$$

$$\tan 2\phi = -\frac{R_3}{R_2}\,. \quad (9)$$

The choice between the plus and minus signs of R is arbitrary. The signs of R_2 and R_3 determine two complementary values of 2ϕ. After fixing η, the resonant Hamiltonian has the form of the harmonic oscillator

$$\mathcal{H} = \alpha J^2 + \beta\cos\psi, \quad (10)$$

with $J \propto S_z$, $\psi = 2\sigma_z + 2\phi$, and $\alpha \simeq -3L_0^{-2}/2 < 0$.

The location of stable equilibrium points depends on the sign of β. If $\beta > 0$, the stable point is at $\psi = 0$, while if $\beta < 0$, the stable point is located at $\psi = \pi$. This means that

$$\begin{aligned} R > 0 &\Rightarrow \omega = k\pi - \phi - \sigma_0 \\ R < 0 &\Rightarrow \omega = \frac{2k+1}{2}\pi - \phi - \sigma_0\,, \end{aligned} \quad (11)$$

where k is integer.

When $\sigma_0 = \pi$, as in the case of the 2 : 3 MMR with Neptune, then $R_2 > 0$ and $R_3 = 0$. In this case, $R > 0$ implies that $\phi = \pm\pi/2$, which gives $\omega = (2k-1)\pi/2$. If, on the other hand, $R < 0$ then $\phi = 0$ and once again $\omega = (2k-1)\pi/2$. These constitute the common libration centers of the Kozai resonance at 90° and 270° (the same result holds for the MMRs with $\sigma_0 = 0$).

If however σ_0 of a MMR is neither 0 nor π, the Kozai resonance does not have libration centers at 90° and 270°. As an example, consider the asymmetric libration center of the 1 : 2 MMR located at $a_0 = 47.797$ AU, $e_0 = 0.383$, and $\sigma_0 = 66.4°$. In this case, $R_2 < 0$ and $R_3 < 0$. If $R > 0$ then $\phi = 329°$ and $\omega = 180k - 35.4°$, while if $R < 0$ then $\phi = 59°$ and $\omega = 90(2k+1) - 125.4°$. The stable centers of the Kozai resonance are at 144.6° and 324.6°, respectively, in good agreement with values observed numerically (Fig. 11).

The choice of initial conditions in our simulation did not guarantee the occurrence of asymmetric librations for $e < 0.13$. The width of the asymmetric island is narrow for small e and all nine particles in the run were initially librating with large A_σ around the symmetric saddle point at 180° (horseshoe orbits). The amplitudes of horseshoe orbits were chaotically changing between 120° and 180°, and only rarely (and for at most several 10^6 yr) did temporary captures in the asymmetric islands occur.

We have performed additional simulations with orbits starting at small e. First, we have found by several trials that permanent tadpole orbits do not exist in practice for $e < 0.07$ (for $e > 0.07$ it is possible to find tadpole orbits that are stable over 4 Byr). Next, we simulated several test particles with initial $e = 0.01$ and 0.05. For each value of e, we have obtained 10 objects showing a resonant behavior, typically alternating between horseshoe orbits and circulation. Their e and i irregularly evolve in the intervals 0–0.2 and 0°–10°, respectively. Interestingly, the irregular motion of some of these test particles was stabilized in a horseshoe regime at $e \sim 0.15$–0.2, $i \sim 5°$–$7°$, and $A_\sigma \sim 100°$. From the test particles with initial $e = 0.01$, only one escaped, while for $e = 0.05$ three particles escaped. This corresponds to the general fact that the orbits starting with initially larger e get destabilized faster by the chaotic eccentricity drift. We estimate that the median lifetime of orbits at $e = 0.05$ in the 1 : 2 MMR is slightly larger than the age of the Solar System. In summary, we found that the resonant space at low e in the 1 : 2 MMR a accounts for about 0.3 AU in a. From 47 resonant test particles simulated with $e < 0.12$ only 8 escaped in 4 Byr, and in this sense, the 1 : 2 MMR is stable in small e. This finding confirms the results of Duncan *et al.* (1995).

4. THE 3 : 4 MMR WITH NEPTUNE

4.1. A Portrait of Regular and Chaotic Dynamics

The only known object in the 3 : 4 MMR with Neptune is 1995 DA2. We have taken this KBO's orbital elements from the Asteroid Orbital Elements Database of the Lowell Observatory.[9] They are reasonably well determined for our purposes because of a relatively large observational arc for this KBO. 1995 DA2 is a counterpart of the asteroid 279 Thule, which is the only stable asteroid discovered until now in the 4 : 3 MMR with Jupiter in the outer asteroid belt. The presence of only one large body in the 4 : 3 Jupiter MMR is puzzling (the diameter of 279 Thule is 135 km), because if the size distribution were similar to the main asteroid belt, there would exist also many small bodies in the resonance (Nesvorný and Ferraz-Mello 1997). On the other hand, the KB is less well known than the asteroid belt and new bodies in the 3 : 4 Neptune MMR may be discovered soon.

[9] The assumed orbital elements of 1995 DA2 on 8/10/1999 (JD 2451400.5) are $a = 36.3396$ AU, $e = 0.074684$, $i = 6.5585°$, $M = 31.836°$, $\omega = 332.008°$, and $\Omega = 127.485°$.

The stability test of the 3 : 4 MMR was performed by the same means as for the 1 : 2 MMR in Section 3. The initial angles of test particles were chosen so that $\sigma_{3:4} = 3\lambda_N - 4\lambda + \varpi = 180^\circ$, $\omega = 90^\circ$, and $\Omega = \Omega_N$. Two sets of initial conditions have been simulated:

(1) 606 test particles with $36 \le a \le 37$ AU ($\Delta a = 0.01$ AU), $e = 0.001$, 0.05, 0.1, 0.15, 0.2, 0.25 (101 test particles for each e), and $i = 5^\circ$; and

(2) 202 test particles with $a = 36.57$ AU, $0 \le e \le 0.3$ ($\Delta e = 0.003$), and $i = 10^\circ$ and 30°. The integration over 10^8 yr was performed by the symmetric multistep method. The planetary configuration, parameters of the simulation, and smoothing routine were the same as for the experiment in the 1 : 2 MMR.

For set (1) of initial conditions, the estimate of the LCE and the minimum distance to Neptune are plotted in Fig. 12. The color coding in Fig. 12 is the same as that used in Fig. 5. Again, we have compensated the scale on the x axes for short-periodic variations of the semi-major axis by a shift of 0.1 AU in a, so that the test particles with the smallest A_σ are near the true resonant center at 36.48 AU.

In Fig. 12, we plot the libration centers and separatrices of the 3 : 4 MMR (bold lines). The Kozai resonance is shown by a thin line (Fig. 12a). We have computed its location from $\dot{\varpi} - \dot{\Omega} = 0$, where the frequencies $\dot{\varpi}$ and $\dot{\Omega}$ were determined as functions of e and a by the semi-numerical method of Henrard (1990). The dashed lines in Fig. 12 show the the 2 : 1 and 3 : 1 commensurabilities between the resonant frequency and the frequency of $\lambda_U - 2\lambda_N$. A pair of two-headed vertical arrows indicates the extrema of the filtered a and e of 1995 DA2 over 10^7 yr (its inclination varies between 1.5° and 8.4°). 1995 DA2 has a resonant orbit with $A_\sigma = 76^\circ$, which is stable on 10^8 yr.

There is a slight asymmetry in the maximum and minimum values of a of 1995 DA2 with respect to the resonant center, which typically happens in the MMRs close to a planet, where the real dynamics differs somewhat from the averaged circular approximation. Nevertheless, the resonant amplitude of 1995 DA2 is clearly small and this object is located in the central regular region of the resonance.

The maximum LCE in the central region of the 3 : 4 MMR is smaller than $\sim 10^{-7}$ yr^{-1} in the interval of 0.3 AU for $e = 0.05$ and of 0.2 AU for $e = 0.1$. The region of small LCE has the size of 0.1 AU for $e = 0.15$, and $\ln \Delta(t)/t$ visibly converges to a nonzero value ($\sim 10^{-6.5}$ yr^{-1}) at $A_\sigma = 0$ for $e \ge 0.2$. The size of the central region we determine here is smaller than that determined by Malhotra (1996) as an extent of regular resonant orbits in a model with Neptune on a circular orbit ($\sim$0.8 AU for $e = 0.1$).

The 3 : 1 three-body resonance is at intermediate A_σ. The corresponding region is clearly chaotic with LCE $\sim 10^{-5.5}$ yr^{-1}. Chaos with the similar LCE value was found in the 4 : 1 three-body resonance inside the 2 : 3 Neptune MMR in N&R00, and it was shown in that paper that moderate chaos generates a slow random walk in A_σ, which in turn can lead to late escapes from the resonance. In this analogy, the orbits in 3 : 1 three-body resonance inside the 3 : 4 Neptune MMR are also potentially unstable. The 3 : 1 resonance should approximately delimit the 30°–40° interval in A_σ of marginally unstable region in the 3 : 4 Neptune MMR.

The minimum distance to Neptune is smaller in the 3 : 4 than in the 1 : 2 (Fig. 5b) and 2 : 3 MMRs (N&R00, their Fig. 2b). It is typically between 5 and 13 AU for the surviving particles. Most particles that approached Neptune at less than $\sim$4 AU subsequently escaped from the resonance.

The determination of δA_σ, δe, and δi shows that the most stable place in the 3 : 4 MMR is at $e = 0.05$, where $\delta A_\sigma = 0.6^\circ$ per 45 Myr for $A_\sigma < 120^\circ$. The expected change of A_σ over 4.5 Byr is 6°. In order to estimate the fraction of objects surviving at $t = 4$ Byr vs A_σ at this eccentricity, we have performed the same experiment as in Section 3.3, modeling the chaotic diffusion as a random walk.

1000 test particles were simulated for each A_σ, and the simulation was repeated for 136 values of A_σ regularly spaced between 0° and 135° for $e = 0.05$ and $i = 5^\circ$. The volume $V(135^\circ)$ occupied by these orbits is 91.4 AU × deg. Assuming the random walk in A_σ, we advanced the orbits of test particles by applying random kicks of the size of δA_σ to their resonant amplitudes. A test particle was removed from the simulation if $A_\sigma > 170^\circ$.

Figure 13 shows the initial density of test particles (dashed line) and the eroded density profile at $t = 4$ Byr (bold line denoted by "+0"). Sixty-eight percent of test particles survived at $t = 4$ Byr. Most escapes occurred for $A_\sigma > 90^\circ$, and for $A_\sigma > 135^\circ$ more than 99% of test particles left the resonance. According to Fig. 13, the maximum density of the current the 3 : 4 MMR population should be at about $A_\sigma \sim 90^\circ$.

The other curves in Fig. 13 show the results of additional experiments adding to δA_σ the evolution of A_σ due to random kicks produced by mutual collisions and dynamical scattering: $\delta A_\sigma^{\rm kick} = 1^\circ$ per 45 Myr (63.5% particles survived), 2° per 45 Myr (58%), and 3° per 45 Myr (53%). The last value shows that $\delta A_\sigma^{\rm kick} > 3^\circ$ per 45 Myr is needed in order to reduce the original population to one-half.

The same reasoning as in Section 3.3 allows us to estimate the ratios of the current numbers of KBOs in the 3 : 4 MMR to those in the 2 : 3 and 1 : 2 MMRs (Eq. (5)). Using $a_{3:4} = 36.48$ AU, $V(135^\circ) = 91.4$ AU × deg, and $P_{\rm surv}^{3:4} = 0.68$, the present number of objects in the 3 : 4 MMR (at $e = 0.05$) should be 77% of the number of the 2 : 3 resonant objects (at $e = 0.2$)[10] and 2.3 times the number of the 1 : 2 resonant objects (at $e = 0.3$). Both of these percentages are in clear contradiction to the observed abundance of the resonant KBOs, implying that the 3 : 4 resonant KBOs must have been efficiently depleted in the early stages of Solar System evolution.

Figure 14 shows the LCEs for set (2) of initial conditions: $i = 10^\circ$ in (a) and $i = 30^\circ$ in (b). The distinctive features are the chaos at $e < 0.05$ (LCE > $\sim 10^{-6}$ yr^{-1}) and regular-like motion

[10] According to Jewitt *et al.* (1996), the observational selection effect is about the same for the 2 : 3 and 3 : 4 MMRs.

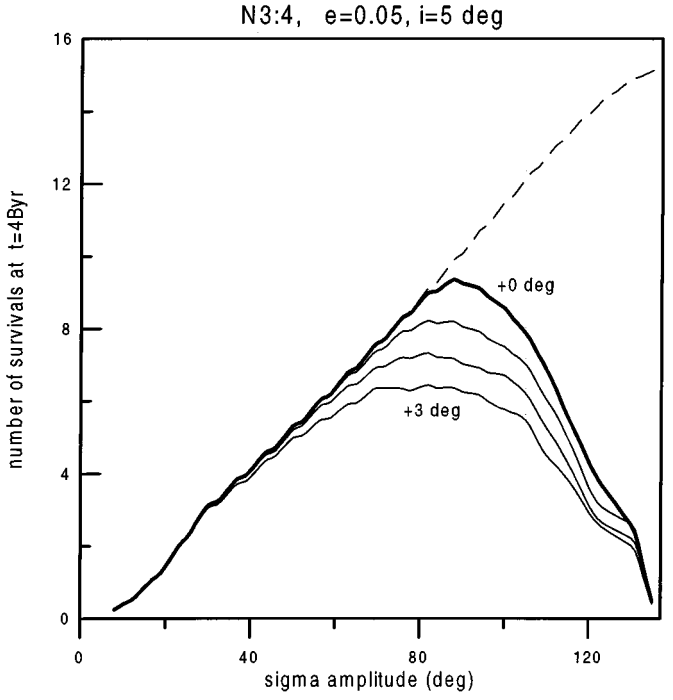

FIG. 13. The number of surviving particles at $t = 4$ Byr in the 3 : 4 MMR ($e = 0.05$ and $i = 5°$) vs initial A_σ. Dashed line shows the initial density distribution. The other lines show the eroded density distributions assuming a random walk at $0 < t < 4$ Byr at a local rate given by $\delta A_\sigma + \delta A_\sigma^{\rm kick}$. The bold line denoted "+0 deg" corresponds to $\delta A_\sigma^{\rm kick} = 0$. The thin lines correspond to values of $\delta A_\sigma^{\rm kick}$ ranging between 1° per 45 Myr and 3° per 45 Myr (denoted "+3 deg").

inside the Kozai resonance ($0.18 < e < 0.23$ for $i = 10°$ and $0.15 < e < 0.25$ for $i = 30°$).

The orbits with small and moderate amplitudes in the Kozai resonance are stable even at large i over the age of the Solar System: $\delta A_\sigma = 0.5°$ per 45 Myr, $\delta e = 0.001$ per 45 Myr, and $\delta i < \sim 1°$ per 45 Myr. Such orbits represent an exception from the general rule found by Duncan *et al.* (1995) that the low-order MMRs in the Kuiper Belt are unstable for $i > 25°$.

4.2. The Long-Term Integration of the 3:4 Resonant Orbits

We performed a long-term integration of 27 test particles initially located in the 3 : 4 MMR. The simulation with `swift_rmvs3` and a time step of 0.5 yr spanned 4 Byr. We have included the perturbations of four major planets with the same initial conditions as in Section 3.4. The test particles initially had $a = 36.735$ AU, $i = 2°$, $0 \le e \le 0.26$ ($\Delta e = 0.01$), $\omega = 90°$, $\Omega - \Omega_{\rm N} = 0$, and $\sigma_{3:4} = 180°$.

For the test particles with $0.02 \le e \le 0.08$, the initial A_σ varied between 20° and 60° (the lower the e, the larger the initial A_σ). These particles move in the ν_{18} secular resonance: the angle $\Omega - \Omega_{\rm N}$ librates around 0 with an amplitude <60°. The amplitude reaches a minimum (30°) for $e \sim 0.06$, which shall correspond to the center of ν_{18} for $i = 2°$ and $A_\sigma \sim 0$. All particles in the interval $0.02 \le e \le 0.08$ survive 4 Byr.

For $e < 0.02$, $\sigma_{3:4}$ alternates between libration with large A_σ and circulation. These orbits are usually unstable over 4 Byr, although they can survive for 2–3 Byr in the resonance before their eccentricities are driven to Neptune-crossing values.

For $e \ge 0.09$ all particles have $A_\sigma < 25°$. These small-A_σ orbits are stable over the age of the Solar System, and most test particles survive the whole simulation without any significant change in their mean A_σ, e, and i. The only exceptions are four particles with initial $e \ge 0.23$, which are ejected from the resonance at $t < 2$ Byr due to close encounters with Neptune. The test particles with $0.19 \le e \le 0.22$ are in the Kozai resonance. The Kozai resonance is narrow for small i and the test particles integrated in this region do not show stable ω librations, but rather alternate between the two centers of the Kozai resonance (90° and 270°) on <∼100 Myr. Stable librations in the Kozai resonance happen at larger i.

The results of this simulation are in general agreement with the resonant portrait presented in the last section. In particular,

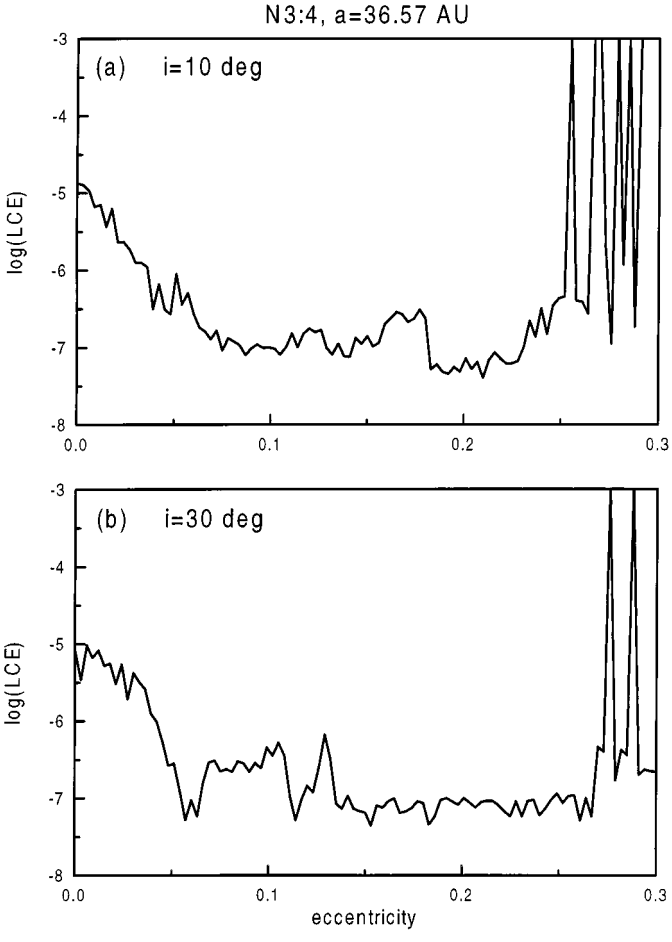

FIG. 14. The LCE for $i = 10°$ (a) and 30° (b) in the 3 : 4 Neptune MMR for $A_\sigma \sim 0$ (set (2) of initial conditions). The largest region with small LCE ($<10^{-7}$ yr^{-1}) is near $e = 0.2$, inside the Kozai resonance. The Kozai resonance enlarges with increasing i, and for $i = 30°$ the interval $0.15 < e < 0.25$ corresponds to practically regular motion.

they verify the existence and extent of the stable core of the 3 : 4 MMR.

5. CONCLUSIONS

We have shown that most chaotic structures in the Kuiper Belt are related to the MMRs with Neptune, three-body resonances with Neptune and Uranus, and MMRs with Uranus (in descending order of importance).

The chaotic evolution of orbits at thin resonances is easy to understand due to its "one-dimensionality": numerical experiments show that orbits evolve in e at almost fixed resonant a, while i changes moderately. The speed of the random walk in e is determined in a complex way by the structure of overlapping resonant multiplets (Nesvorný and Morbidelli 1999) and developing a satisfactory theoretical model is an issue for future studies.

The existence of a resonant-driven random walk in e changes the common view that the minor body belts are "frozen" in regions sufficiently distant from the main MMRs and secular resonances, and suggests that the structure of these belts is time-dependent, with substantial eccentricity evolution. Apart from widely discussed consequences—as the mechanism of supply of transient populations of planets-crossers (ecliptic comets from the KB and Earth-crossers from the inner asteroid belt)—we believe that thin MMRs are ideal places for testing today's models of collisional, scattering, and dissipative evolution in the belts. Indeed, a large percentage of the current population at thin MMRs should have been collisionally injected, and the detection of "mini-gaps" (or failure to detect them) at thin MMRs can provide constraints on the injection probabilities. Such a study is more appropriate for asteroids, whose orbital distribution is better known.

The chaotic evolution in large MMRs is more complex and is determined by the structure of inner secular, secondary, and three-body resonances. We have investigated the first-order 1 : 2, 2 : 3 (in N&R00), and 3 : 4 MMRs with Neptune. This study has confirmed the findings of Duncan *et al.* (1995) and Morbidelli (1997) that the chaotic evolution in MMRs dominantly affects A_σ (or equivalently, the amplitude of a) and that the above resonances have stable "cores" for small A_σ, where all orbits survive 4×10^9 yr. This stable core is substantially smaller in the 1 : 2 than in the other two MMRs. The approximate limits of stable motion at small i are $0.15 < e < 0.35$ and $A_\sigma < 30^\circ$ in the 1 : 2 MMR, $0.05 < e < 0.25$ and $A_\sigma < 100^\circ$ ($A_\sigma < 50^\circ$ for $e = 0.3$) in the 2 : 3 MMR, and $0.03 < e < 0.2$ and $A_\sigma < 80^\circ$ in the 3 : 4 MMR. The most regular motion for large inclinations occurs inside the Kozai resonance at $e \sim 0.25$ in the 2 : 3 MMR, at $e \sim 0.2$ in the 3 : 4 MMR, and in the interval $0.2 < e < 0.27$ in the 1 : 2 MMR. These orbits are stable over the age of the Solar System.

The stable resonant cores are enclosed by the marginally unstable regions where a percentage of objects escape from resonances over the age of the Solar System (Duncan *et al.* 1995, Morbidelli 1997). This region is typically 20°–40° wide in A_σ. In the case of the 2 : 3 resonance, the marginally unstable region is at the place of the 4 : 1 three-body resonance. In addition to thin MMRs outside the 2 : 3 MMR, it is this 4 : 1 three-body resonance that generates a significant number of the present Neptune-crossers. The marginally unstable region in the 3 : 4 MMR with Neptune generated by the 3 : 1 three-body resonance.

The evolution of e is important in the strongly unstable region at large A_σ. The alternation between resonant libration and circulation produces a fast random walk of e. It takes at most several 10^8 yr to drive an orbit from the small e to Neptune-crossing orbit by this mechanism.

We have determined the number of currently known KBOs on resonant orbits stable over 4 Byr. There is 1 such body in the 3 : 4 MMR (1995 DA2), 15 bodies and Pluto in the 2 : 3 MMR, and probably 2 objects in the 1 : 2 MMR.

The current best-fit orbital elements of 1997 SZ10 and 1996 TR66 do not correspond to the stable resonant motion in the 1 : 2 Neptune MMR. While for 1997 SZ10 they indicate an unstable horseshoe orbit, the current orbital elements of 1996 TR66 place this object on a nonresonant orbit. Conversely, the orbital angles of these KBOs suggest they are resonant bodies. Indeed, the angles $\sigma_{1:2}$ of 1997 SZ10 (-69°) and 1996 TR66 (-62°) are surprisingly close to the center of the asymmetric librations for $e = 0.37$: $\sigma_0 \sim 67^\circ$, which is likely not a mere coincidence. 1997 SZ10 and 1996 TR66 are most probably dynamically primordial objects in the 1 : 2 MMR that currently librate with small A_σ on stable orbits. We believe that future improvement of their orbital elements will confirm this conjecture. Neverthless, as we have discussed in Section 2.1, our probabilistic argument in favor of this hypothesis cannot completely exclude the possibility that 1997 SZ10 and 1996 TR66 are temporarily captured objects from the scattered disk.

We have estimated that, if eccentricities have been efficiently uniformized by the primordial excitation at resonances, then the current number of objects at the most stable places the resonances ($e = 0.3$ for 1 : 2, $e = 0.2$ for 2 : 3, and $e = 0.05$ for 3 : 4) shall be roughly in the ratio $N_{1:2} : N_{2:3} : N_{3:4} = 2 : 6 : 5$, while the observed apparent ratio is 2 : 16 : 1. Correcting the apparent ratio for the observational selection effects (Jewitt *et al.* 1998), the estimated current population of the 2 : 3 and 1 : 2 MMRs agrees roughly with the above theoretical prediction. Conversely, the 3 : 4 MMR with Neptune must have been significantly depleted in the early phases of the Solar System evolution.

ACKNOWLEDGMENTS

This research was sponsored by the São Paulo State Science Foundation FAPESP. Some of the numerical simulations were performed using the facilities of the São Paulo University computer center LCCA in the frame of the project "Asteroid resonant dynamics and chaos." We are indebted to Harold Levison for a very helpful referee report. We thank Brett Gladman for language corrections.

Note added in revisions. We recently learned about the recovery of 1997 SZ10 (B. Gladman, personal communication), which allowed for better determination of its orbit (B. Marsden, personal communication). While the eccentricity and the angular orbital elements stayed basically unchanged with respect to the previous determination (eccentricity changes by 0.005 and angles by less than 1.5°), the semi-major axis came down to 48.411 AU. This is exactly what we

have anticipated in this work. The 0.26-AU change of the semi-major axis places 1997 SZ10 very close to the libration center of the 1 : 2 MMR. We found in an additional simulation that these new orbital elements of 1997 SZ10 correspond to an initially resonant orbit starting with $A_\sigma \sim 30^\circ$ in the tadpole regime. In the meantime, 1996 TR66 still awaits for a recovery that would improve its orbital determination.

REFERENCES

Beaugé, C. 1994. Asymmetric librations in exterior resonances. *Celest. Mech. Dynam. Astron.* **60**, 225–248.

Benettin, G., L. Galgani, and J. M. Strelcyn 1976. Kolmogorov entropy and numerical experiments. *Phys. Rev. A* **14**, 2338–2345.

Duncan, M. J., and H. F. Levison 1997. A disk of scattered icy objects and the origin of Jupiter-family comets. *Science* **276**, 1670–1672.

Duncan, M. J., H. F. Levison, and S. M. Budd 1995. The dynamical structure of the Kuiper belt. *Astron. J.* **110**, 3073–3081.

Gallardo, T., and S. Ferraz-Mello 1998. Dynamics in the exterior 2 : 3 resonance with Neptune. *Planet. Space Sci.* **46**, 945–965.

Gladman, B., J. J. Kavelaars, J.-M. Petit, A. Morbidelli, M. J. Holman, and T. Loredo 2000b. The structure of the Kuiper belt: Size distribution and the radial extent. *Astron. J.*, submitted for publication.

Gladman, B., J.-M. Petit, and M. Duncan 2000a. Does Pluto affect the trans-neptunian region? In *Minor Bodies in the Outer Solar System* (R. West, Ed.). Kluwer Academic, Dordrecht, in press.

Hahn, J. M., and R. Malhotra 1999. Orbital evolution of planets embedded in a planetesimal disk. *Astron. J.* **117**, 3041–3053.

Henrard, J. 1990. A semi-numerical perturbation method for separable Hamiltonian systems. *Celest. Mech. Dynam. Astron.* **49**, 43–67.

Holman, M., and N. Murray 1996. Chaos in high-order mean resonances in the outer asteroid belt. *Astron. J.* **112**, 1278–1293.

Jewitt, D., J. Luu, and J. Chen 1996. The Mauna Kea–Cerro Tololo (MKCT) Kuiper belt and Centaur survey. *Astron. J.* **112**, 1225–1238.

Jewitt, D., J. Luu, and C. Trujillo 1998. Large Kuiper belt objects: The Mauna Kea 8K CCD survey. *Astron. J.* **115**, 2125–2135.

Knežević, Z., A. Milani, P. Farinella, Ch. Froeschlé, and C. Froeschlé 1991. Secular resonances from 2 to 50 AU. *Icarus* **93**, 316–330.

Laskar, J. 1994. Large-scale chaos in the Solar System. *Astron. Astrophys.* **287**, L9–L12.

Laskar, J. 1999. Introduction to frequency map analysis. In *Hamiltonian Systems with Three or More Degrees of Freedom* (C. Simó, Ed.), pp. 134–150. Kluwer, Dordrecht.

Levison, H. F., and M. Duncan 1994. The long term behavior of short-period comets. *Icarus* **108**, 18–36.

Malhotra, R. 1995. The origin of Pluto's orbit: Implications for the Solar System beyond Neptune. *Astron. J.* **110**, 420–429.

Malhotra, R. 1996. The phase space structure near Neptune resonances in the Kuiper belt. *Astron. J.* **111**, 504–516.

Malhotra, R. 1997. Implications of the Kuiper belt structure for the Solar System. In *ACM Conference 1996, Versailles, France.* Unpublished.

Migliorini, F., P. Michel, A. Morbidelli, D. Nesvorný, and V. Zappalà 1998. Origin of Earth-crossing asteroids: A quantitative simulation. *Science* **281**, 2022–2024.

Milani, A., and A. Nobili 1992. An example of stable chaos in the Solar System. *Nature* **357**, 569–571.

Morbidelli, A. 1996. The Kirkwood gap at the 2/1 commensurability with Jupiter: New numerical results. *Astron. J.* **111**, 2453–2461.

Morbidelli, A. 1997. Chaotic diffusion and the origin of comets from the 2/3 resonance in the Kuiper belt. *Icarus* **127**, 1–12.

Morbidelli, A. 1998. The structure of the Kuiper belt and the origin of Jupiter-family comets. In *Solar System Formation and Evolution* (D. Lazzaro, R. Vieira Martins, S. Ferraz-Mello, and C. Beaugé, Eds.), pp. 83–105. ASP Conference Series 149, San Francisco.

Morbidelli, A., and D. Nesvorný 1999. Numerous weak resonances drive asteroids toward terrestrial planets orbits. *Icarus* **139**, 295–308.

Morbidelli, A., F. Thomas, and M. Moons 1995. The resonant structure of the Kuiper belt and the dynamics of the first five trans-neptunian objects. *Icarus* **118**, 322–340.

Murray, N., and M. Holman 1997. Diffusive chaos in the outer asteroid belt. *Astron. J.* **114**, 1246–1259.

Murray, N., M. Holman, and M. Potter 1998. On the origin of chaos in the asteroid belt. *Astron. J.* **116**, 2583–2589.

Nesvorný, D., and S. Ferraz-Mello 1997. On the asteroidal population of the first-order jovian resonances. *Icarus* **130**, 247–258.

Nesvorný, D., and A. Morbidelli 1998. Three-body mean motion resonances and the chaotic structure of the asteroid belt. *Astron. J.* **116**, 3029–3037.

Nesvorný, D., and A. Morbidelli 1999. An analytic model of three-body mean motion resonances. *Celest. Mech. Dynam. Astron.* **71**, 243–271.

Nesvorný, D., and F. Roig 2000. Mean motion resonances in the trans-neptunian region. I. The 2 : 3 resonance with Neptune. *Icarus* **148**, 000–000.

Nesvorny, D., F. Roig, and S. Ferraz-Mello 2000. Close approaches of transneptunian objects to Pluto have left observable signatures on their orbital distribution. *Astron. J.* **119**, 953–969.

Nobili, A., A. Milani, and M. Carpino 1989. Fundamental frequencies and small divisors in the orbits of the outer planets. *Astron. Astrophys.* **210**, 313–336.

Petit, J. M., A. Morbidelli, and G. Valsecchi 1999. Large scattered planetesimals and the excitation of the small body belts. *Icarus* **141**, 367–387.

Quinlan, G., and S. Tremaine 1990. Symmetric multistep methods for the numerical integration of planetary orbits. *Astron. J.* **100**, 1694–1700.

Roig, F., A. Simula, S. Ferraz-Mello, and M. Tsuchida 1998. The high-eccentricity asymmetric expansion of the disturbing function for non-planar resonant problems. *Astron. Astrophys.* **329**, 339–349.

Šidlichovský, M., and D. Nesvorný 1999. A study of chaos in the asteroid belt. In *The Dynamics of Small Bodies in the Solar System: A Major Key to Solar System Studies* (B. Steves and A. E. Roy, Eds.), pp. 31–36. Kluwer, Dordrecht.

Tremaine, S. 1990. Dark matter in the Solar System. In *Baryonic Dark Matter* (D. Lynden-Bell and G. Gilmore, Eds.), pp. 37–65. Kluwer, Norwell, MA.

Valsecchi, G., and A. Manara 1997. Dynamics of comets in the outer planetary region II. Enhanced planetary masses and orbital evolutionary paths. *Astron. Astrophys.* **323**, 986–998.